Chapter-2

2.1 Introduction

Core and linker histone proteins form the major class of nuclear proteins that condense the genome into a highly organized chromatin assembly within living cells **[1]**. The dynamic removal and reassembly of histones and their variants are considered essential in the maintenance of epigenetic memory **[2]**. The functional roles of core and linker histones are found to be distinct, arising due to their differential nature of DNA association. While the core histones with their epigenetic modifications play a central role in regulating access to DNA **[3]**, the linker histones (with other non-histone proteins) are thought to participate in maintaining the dynamic higher order chromatin structure **[4]**. Although some of the linker histone variants play a role in somatic development **[5]**, the implicit roles of linker histones remain unclear **[6]**. Since histones are found to be regulators of cellular processes, understanding their *invivo* dynamics in the context of chromatin organization and nuclear architecture has become important.

Recent progress in fluorescence-based live-cell monitoring techniques **[7]** and modifying histone proteins with GFP fusion proteins **[8]** have provided new means to study their mobility within the nucleus. These studies have revealed that the core and linker histones that package the genome are highly dynamic within living cells. Using fluorescence anisotropy experiments we have shown **[9]** that core and linker histone proteins form a distinct heterogeneous structure inside a live cell nucleus. The chromosomal compaction map strongly depends upon state of the cell and takes an important role in maintaining the epigenetic state of the cell nucleus. The significant fraction of the freely diffusing core and linker histones is important for the chemical modification of the chromatin fiber and hence the maintenance of the epigenetic state of the cell nucleus.

Our fluorescence anisotropy experiments show that the chromatin structure is heterogeneous and is differentially compacted in different parts of the cell nucleus. Photo-bleaching experiments coupled to fluorescence anisotropy experiments indicate a significant fraction of freely diffusing core histone inside

the chromatin fiber. The nature of core and linker histone diffusion and their influence on local chromatin assembly within living cells have been explored quantitatively. The hindrance to histone mobility offered by the heterogeneous chromatin assembly is poorly understood. Using experiments with single molecule resolution and numerical simulations, I have tried to understand the nucleosomal fluidity, the diffusive mechanisms of different core and linker proteins and their functional localization within live cells.

2.2 Mapping nucleosome fluidity in live cell nuclei

Fluorescence anisotropy has been used to understand the nucleosomal fluidity inside the live cell nuclei. For this, polytene chromosomes derived from the *Drosophila* salivary gland cells, with core histone (H2B) fused with Enhanced Green Fluorescent Protein (H2B-EGFP) are used as the model system. In all these experiments, live single cell fluorescence visualization in conjunction with anisotropy imaging gives a map of the steady state rotational dynamics of nucleosomes (H2B) and thus a measure of their fluidity within the cell nucleus. This method also gives us a handle on the distinct and heterogeneous nucleosome fluidic domains on the genome. The experimental data show that H2B proteins exist as both bound and unbound fractions inside the cell nucleus.

2.2.1 Methods

Confocal Fluorescence Imaging & Fluorescence Anisotropy

A Zeiss Confocor (Model- LSM510/Confocor 2) fluorescence microscope equipped with fluorescence anisotropy imaging is used in our experiments. Imaging (including anisotropy imaging) is carried out using Plan Apochromat 63 X/ 1.4 NA oil immersion microscope objective. Confocal images (512 X 512 pixels, 12 bit images, pinhole aperture size ~ 1 airy-unit) are acquired using 488 nm excitation from an Argon-Ion laser and 515 ± 30 nm band pass emission filter for EGFP. Typical time for one image-acquisition is about a second with

optimized instrumental settings. For anisotropy images, the parallel (I_{II}) and perpendicular ($I_{\perp}$) components of the emitted light (with respect to polarized excitation) are simultaneously acquired, as above, ensuring that both the detectors have similar optimized settings. From the components of parallel and perpendicular intensity fluorescence emission we can calculate the steady state fluorescence anisotropy as $r = \frac{I_{II} - I_{\perp}}{I_{II} + 2I_{\perp}}$. In steady state measurements, the anisotropy follows the Perrin's equation $r = r_0/(1+\tau RT/\eta V)$, where r_0 is the value at $t = 0$, τ is the fluorescence life time of the fluorophore, η is the local viscosity and V is the hydrodynamic radius. In these experiments, the dependence of r as a function of η (the viscosity) gives a measure of the average local fluidity of the fluorophores **[10]**.

In order to quantify the anisotropy values, wide-field anisotropy images were captured on a NIKON/OLYMPUS microscope with 100X/1.4 NA objective and images captured with ICCD cameras (Roper Scientific). Mercury Arc-lamp is used for the excitation light which is then selected for vertical polarization using a sheet polarizer (Melles Griot). The light collected is split into its parallel and perpendicular polarization components using a polarizing beam splitter (Melles Griot) or by swapping between two polarizers (Melles Griot) parallel and perpendicular to the excitation. Images are captured using V++ Digital Optics software and analyzed using LabView.

2.1.2 Model System

Salivary gland cells containing the polytene chromosomes, derived from the *Drosophila* larvae, are used as a model system. The C terminal sequence of the histone proteins (H2B) is genetically tagged with a reporter gene coding for Enhanced Green Fluorescent Protein (EGFP). The salivary glands, from the 3rd instar larvae, are dissected in Ringers medium using standard protocols **[11].** The glands are transferred onto a clean microscope #1 coverslip in the Ringers medium

and sealed using another coverslip. Care is taken to ensure that the glands are intact during the sample preparation procedure and the samples are stable for microscopic observations

2.2.3 Results

(i). Imaging nucleosome fluidity using fluorescence anisotropy.

Figures 2.2.2-a,c, show the confocal fluorescence and anisotropy images of a salivary gland cell nucleus. H2B fused with EGFP provides a direct visualization of the intact polytene chromosome. From the fluorescence images, the band and the non-band regions of the polytene chromosome can be easily identified. The images are acquired with ~ 64 μsec pixel time. The anisotropy images are calculated from the fluorescent images collected in the parallel and the perpendicular direction. The measured anisotropy values per pixel directly track the rotational degrees of freedom of the H2B-EGFP protein and thus map the fluidity of the histone-DNA (nucleosome) complex. The dark regions in the anisotropy images correspond to higher values of anisotropy. The compact form of the chromosome regions shows a higher anisotropy value in contrast to less compact regions. **Figure-2.2.2-e**, is a plot of the distribution of the normalized anisotropy values which shows that the different regions of the chromosome have large variations in nucleosome fluidity depicting their spatio-temporal variation in compaction. Interestingly, the distribution is non-gaussian with a large standard deviation. We suggest that the skewed distribution in anisotropy values represents the distinct compaction states of the H2B-EGFP proteins bound to the chromosome, thereby providing a probe of mapping chromatin structures. In **Figure-2.2.2-b,d**, the intensity and anisotropy images of samples prepared in Ringers medium with 600 mM NaCl are also presented in order to elucidate the nature of nucleosome compaction. It is known that above 400 mM NaCl, nucleosomes begin to disassemble from the compact chromosomal structure **[12,**

13]. As can be clearly seen in **Figure-2.2.2**, the width of the anisotropy distribution values, under 600 mM salt conditions, has a much smaller standard deviation with Gaussian distribution around the normalized mean. From our imaging studies, we clearly observe that the anisotropy values are strongly dependent on the intensity values.

(ii) Wide field anisotropy images show distinct euchromatin and heterochromatin organization.

We have used wide-field fluorescence anisotropy imaging with highly sensitive camera to understand distinct packaging in the euchromatin and heterochromatin regions as well as to get the numerical value of fluorescence anisotropy [9]. The anisotropy images are calculated from individual parallel and perpendicular polarized images ($r = \frac{I_{\parallel} - I_{\perp}}{I_{\parallel} + 2I_{\perp}}$) and plotted with color coding to differentiate various levels of fluidic regions. Highly fluidic regions (lower anisotropy) are violet to blue in color and compacted regions are white (higher anisotropy). For all the above experiments we have ensured that the changes in anisotropy values are not an artifact of variations in fluorescence intensity values. Using polytene chromosomes from *Drosophila* larvae salivary glands, we demonstrate (**Figure 2.2.3-a)** that anisotropy can distinguish between the two states of chromatin assembly showing distinct band and interband regions **[11]**. The corresponding distribution of anisotropy of an internal region (**Figure-2.2.3-b**) exhibits a clear bimodal distribution confirming the existence of spatially separated euchromatin (first peak) and heterochromatin (second peak). In a high salt environment (600mM NaCl) due to screening of electrostatic interactions, the chromatin higher order structure is known to breakdown. Under such conditions we find the disappearance of bands (**Figure-2.2.3-a inset**) and an overall reduction of the mean anisotropy (**Figure-2.2.3-b inset**) indicating global decondensation of the chromatin and thereby further confirming compaction measurements by fluorescence anisotropy.

(iii). Fluidity of bound and unbound fractions of H2B proteins using photo bleaching.

In order to probe the origin of the variability of anisotropy values and its dependence on intensity, photobleaching experiments were carried out. **Figure 2.2.4-a, b**, shows the plots of the intensity and anisotropy vs. time in Ringer's medium at 150 mM (physiological) & 600 mM NaCl concentrations. For these experiments, the home-built confocal anisotropy detection setup with fast data acquisition was used **[10]**. The typical confocal spot (~300 nm diameter) is much smaller than the chromosome arm. The data is obtained by simultaneously recording both the intensity and anisotropy values as a function of time. The intensity decay data fits well to a single time scale (600 mM NaCl) but interestingly to two distinct time scales at 150 mM NaCl. Typical timescale obtained from the fit (function for single time scale) is 12 ± 2.35 Sec (600 mM NaCl) and from the two-time scale fitting function $I = \left[I_1 \exp\left(-t/\tau_1\right) + I_2 \exp\left(-t/\tau_2\right)\right]$ are 2.03 ± 0.94 Sec and 19.6 ± 7.41 Sec (at 150 mM NaCl). In addition, at 150 mM, the anisotropy values decreases with bleaching time while it is constant for the case of 600 mM NaCl. Our results lead us to suggest the presence of bound and free fraction of H2B-EGFP in the observation volume. The bound fraction has a larger anisotropy compared to the unbound fraction, which is free to diffuse. Upon fluorescence excitation, the bound fraction bleaches much faster than the free ones as can be clearly seen in the two time scale fits to the intensity decay curves. In contrast, the photobleaching experiments in 600 mM NaCl show the presence of only the unbound fraction within the cell nucleus as seen by a single time scale fit to the data. In **Figure 2.2.4**, we plot the anisotropy vs. intensity values for both the cases. The anisotropy values decrease non-linearly with reduction in intensity for 150 mM, while remaining independent of intensity for 600 mM. In order to understand these results, we use a simple phenomenological function $r = \left[\dfrac{\exp\left(-t/\tau_f\right)\cdot r_f + A\cdot\exp\left(-t/\tau_b\right)\cdot r_b}{\exp\left(-t/\tau_f\right) + A\cdot\exp\left(-t/\tau_b\right)}\right]$ to fit the data where r is the anisotropy, τ

is the bleaching time scale and the subscript b and f corresponds to the bound and free fractions respectively. Except the free parameter "A" which denotes the ratio of the intensity contributions of the bound and free particles at time t=0, all other parameters in this function are experimentally determined using the photo bleaching and anisotropy experiments, as described above. The fit to the experimental data is shown in **Figure 2.2.4** as the solid line. The qualitative agreement between the experiments and the phenomenological function suggests the presence of free and bound H2B-EGFP proteins in the chromosome segment regions.

Figure 2.2.1

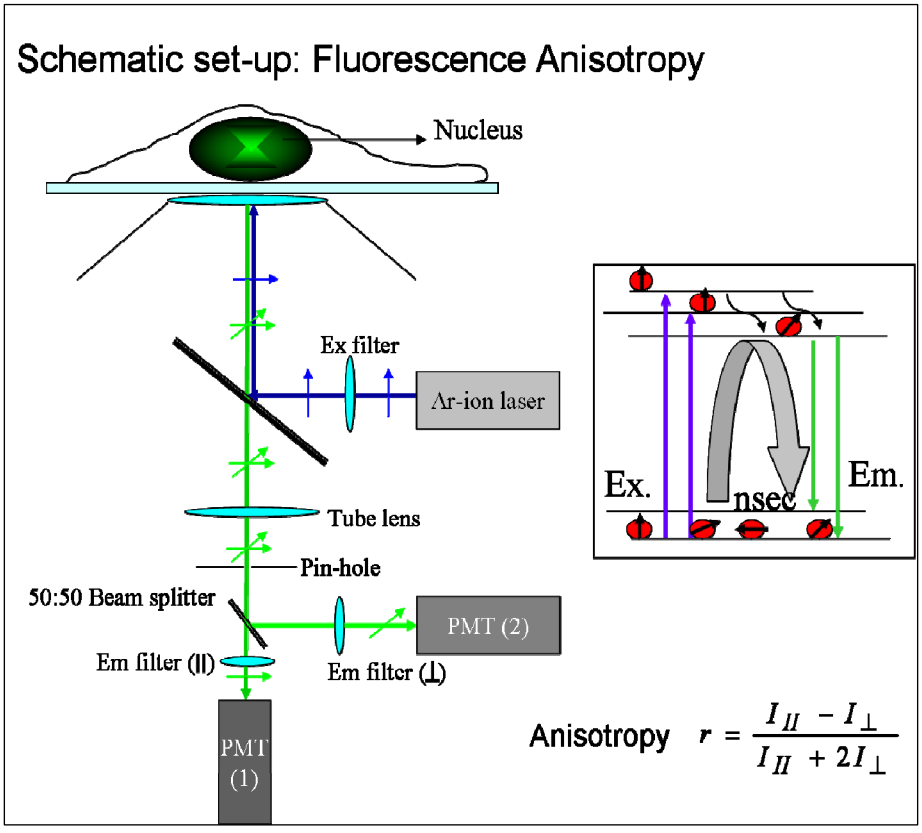

Figure 2.2.2

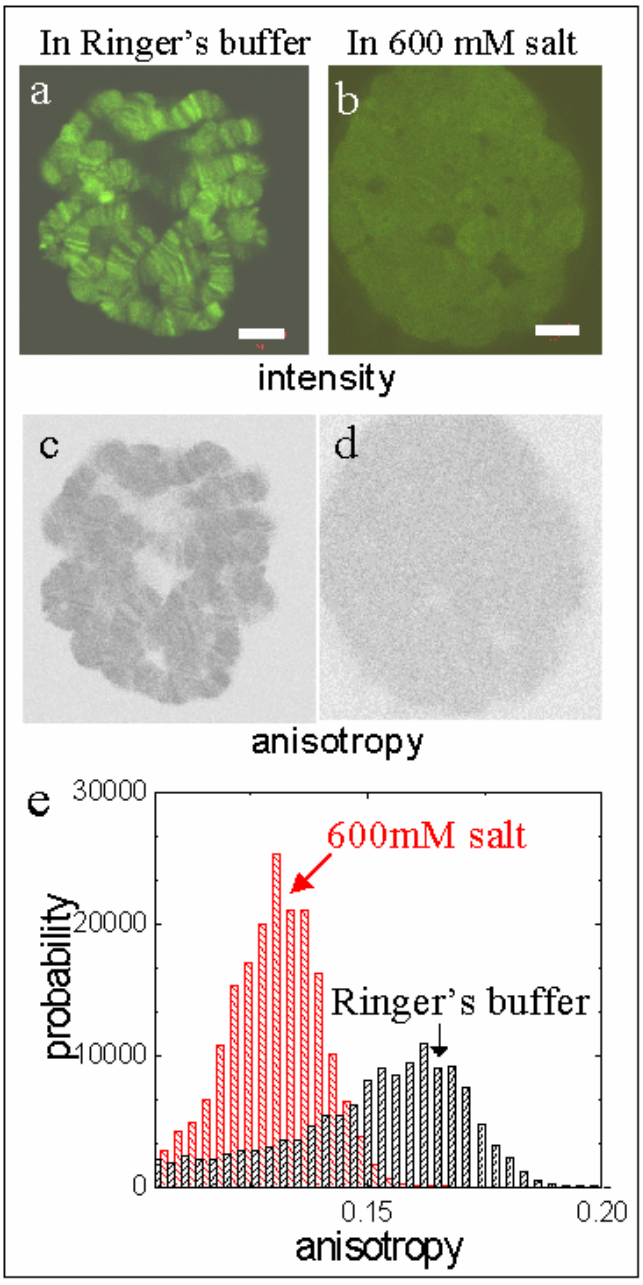

Confocal fluorescence image of polytene chromosome with H2B fused to EGFP: (a) in Ringer's medium and (b) in 600 mM NaCl buffer. Corresponding fluorescence anisotropy images (c) in Ringer's medium and (d) in 600 mM NaCl buffer. Scale bar = 5 μm (e) Pixel wise anisotropy distribution.

Figure 2.2.3

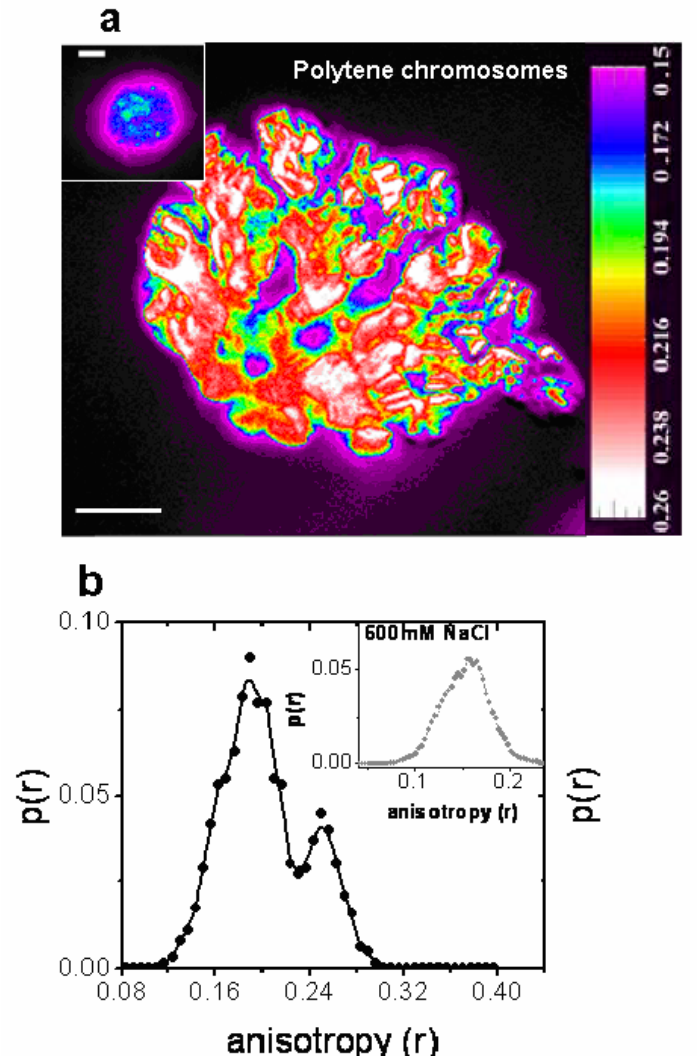

Chromatin compaction maps by fluorescence anisotropy imaging. Color-coded anisotropy map of (a) polytene chromosomes extracted from salivary glands of *Drosophila* larvae; inset: polytene chromosomes in 600mM NaCl;

(b) The fluorescence anisotropy distribution of polytene cell indicates distinct chromosomal compaction in different parts of the chromosomal arms. Inset: the anisotropy distribution of the polytene chromosome treated with 600mM salt (NaCl). The mean and the SD of anisotropy distribution decreases with salt induced decondensation.

Figure 2.2.4

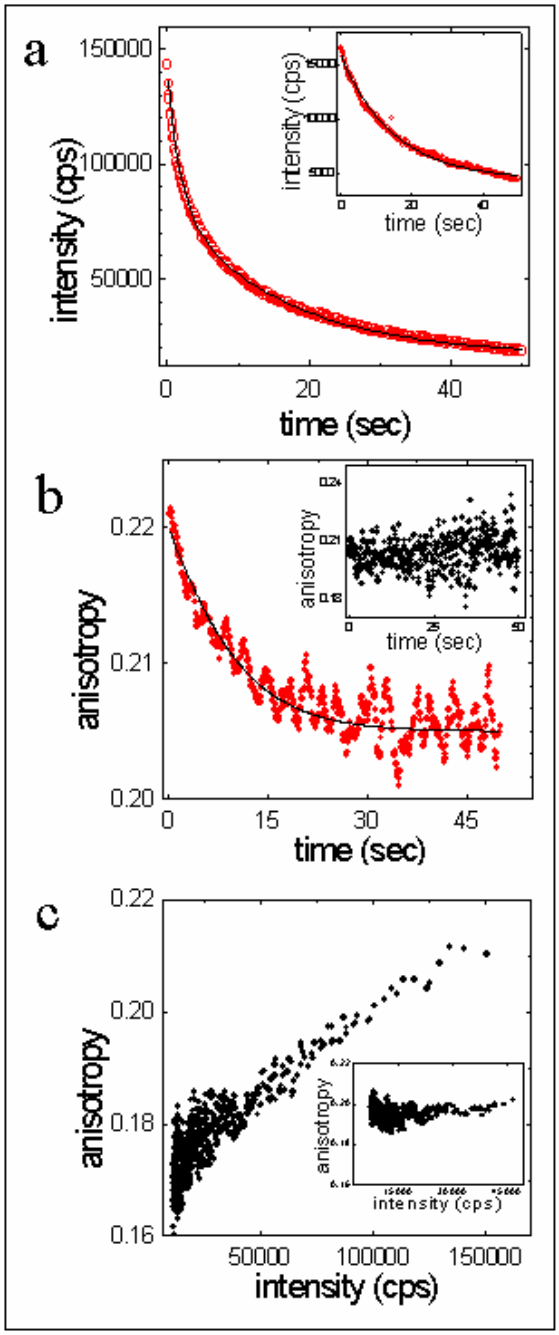

Change in anisotropy with photo bleaching in Ringer's medium. (a) Intensity decay with double exponential fit (solid line). (b) Anisotropy decay with the phenomenological fit (solid line) (c) anisotropy vs. intensity plot. Inset to a,b & c, corresponding results in 600mM NaCl buffer.

Figure 2.2.5

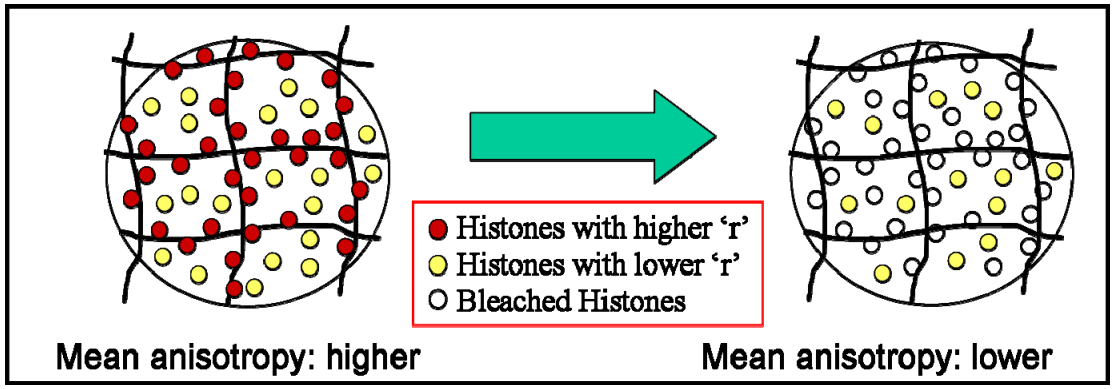

Schematic model to understand the decrease in fluorescence anisotropy due to photo-bleaching.

Using fluorescent anisotropy imaging, I have shown that distinct nucleosomal fluidity exists in different parts of the chromosome in *Drosophila* larvae salivary gland cells. At 600 mM NaCl, the fluorescence anisotropy values decrease, pointing to a less condensed structure when compared to the chromosome in physiological conditions. Fluorescent anisotropy coupled with photobleaching experiments indicates a significant percentage of freely diffusing fraction of the core histones in the salivary gland cell nucleus.

2.3 Core and linker histones diffusion measurements

2.3.1 Methods

(i). Plasmid Construction

The H2B-EGFP expressing pBOS plasmid was gifted to us by Kanda et al. Human H4-EGFP plasmid was made in two steps. The gene was first amplified from HeLa genomic DNA using primers (X60483, H4-fwd: 5'GGGGTACCATGTCTGGCC GCGG 3'and H4-rev: 5' CGGGATCCCCACCGAAACCGTAGAG 3'), was digested and ligated into pBOS-H2B-EGFP using *Kpn* I and *Bam* HI restriction sites. Then the *Bam* HI-EGFP-*Not* I fragment from the resulting plasmid was replaced with a *Bgl* II–EGFP-*Not* I fragment from pEGFP N1 (Clontech) plasmid, in order to generate a 23 amino acid residue linker between H4 and EGFP, driven by an Elongation Factor (EF) 1α Promoter. Human H1.1 gene, driven by CMV promoter, was amplified from HeLa genomic DNA using primers

(X57130; H1.1-fwd: 5' GGGGGATCCATGTCTGAAACAGTGCCTC 3'

and H1.1-rev: 5' AAAACCGGTTTCTTGGGTGCCGCTTTC 3') and cloned into pEGFP N1 vector using *Bam* HI and *Age* I restriction sites. Human H1.2 & H1.4 genes were amplified from HeLa genomic DNA using primers

(X57129; H1.2-fwd: 5' GGGGTACCATGTCC GAGACTGCTCCTG 3';

H1.2-rev: 5'CGGGATCCCGTTTCTTCTTGGGCG3'

and M60748; H1.4-fwd: 5'GGGGTACCATGTCCGAGACTGCGCC3';

H1.4-rev: 5'CGGGATCCTTTTTCTTGGCTGCCGC 3') and cloned into pEGFP N1 vector using *Kpn* I and *Bam* HI restriction sites. Human H1.5 gene was also amplified from HeLa genomic DNA using primers

(X83509;H1.5-fwd:5'GGGGTACCATGTCGGAAACCGC3';

H1.5-rev:5'CGGGATCCT TCTTTTTGGCAGCC3')

and ligated into pEGFP N1 vector at *Bam* HI site on the 3' end and a blunt end on the 5' end. The tailess H1.1 was constructed by screening for the core domains of the proteins using the Conserved Domain Search database (http://www.ncbi.nlm.nih.gov/Structure/cdd/wrpsb.cgi) and then amplifying the core domains alone. The tailess H1.1 gene was amplified from pH1.1 - EGFP N1 by using primers

(tailessH1.1-fwd: 5'GGGGGATCCATGTCCGTGTCAGAGC3';

tailessH1.1- rev: 5'AAAACCGGTTTGGTTTCCACGGAGG 3') and cloned into pEGFP N1 using *AgeI* and *Bam HI* restriction sites.

(ii). Cell Culture

HeLa cells were cultured in Dubelco's Minimum Eagle Medium (DMEM) (Gibco) supplemented with 10% foetal bovine serum (FBS) (Gibco) and penicillin-streptomycin (Gibco), in a 5% CO_2 incubator. HeLa WT cells were transfected with 200ng of DNA using Lipofectamine 2000 (Invitrogen). Stable cell lines expressing H2B-EGFP were generated using selection by Blasticidin. ATP depletion was realized by incubating cells for one hour with 6 mM 2-deoxy-D-glucose and 10 mM sodium-azide in medium1 buffer at 37^0C.

Plasmids expressing different fluorescently tagged core and linker histones were transfected with lipofectamine-2000 (Invitrogen). A concentration of 1μg of DNA was used for each transfections using standard transfection protocols. Transfected cells were observed under fluorescence microscope and incubated in 37 degree 5% carbon –di-oxide incubator. The transfected cells were selected by G418 and stable clones were sorted using a fluorescence sorter (Becton Dickenson).

Salivary gland cells (with polytene chromosomes), derived from the *Drosophila* larvae (transgenic flies bearing histone C-terminal H2B fused to EGFP (unknown source)), were used. The salivary glands, from the 3rd instar larvae, were dissected in Ringer's medium (or, medium containing 600 mM NaCl for control experiments) using standard protocols. The middle portion of the larvae is held using one micro-needle under an inspection microscope. Another fine tipped forceps is used to pull out the mouth region of the larvae. The salivary glands are dissected using the protocol mentioned above. The glands are then transferred onto a clean microscope #1 coverslip in the Ringer's medium and sealed using another coverslip. Care is taken to ensure that the cells are intact during the sample preparation procedure and the samples are stable for microscopic observations.

(iii). Fluorescence Microscopy & FRAP experiments

All imaging experiments were done in Medium1 buffer (150mM NaCl, 5mM KCl, 1mM $CaCl_2$, 1mM $MgCl_2$, 20mM HEPES, pH 7.3), supplemented with 1 % glucose, except in ATP depletion experiments. A Zeiss Confocor (Model-LSM510-Meta/Confocor2) fluorescence microscope equipped with fluorescence correlation spectroscopy was used in our experiments. For imaging, FRAP and FCS experiments, we used a C-Apochromat 40X/ 1.2 N.A water corrected objective. Confocal images (512 X 512 pixels, 12 bit images, pinhole aperture size ~ 1 airy-units) were acquired. EGFP and its fusion proteins were excited with the 488 nm line of an Argon-ion laser (Lassos) and the emission collected with a 500-530 nm band pass filter.

(iv). Fluorescence Correlation Spectroscopy

In FCS experiments, the correlation of the time course of intensity fluctuations of the fluorescence signal I (t) was measured. From the intensity time series the autocorrelation function, $G(\tau) = \frac{\langle I(t+\tau).I(t)\rangle - \langle I^2(t)\rangle}{\langle I^2(t)\rangle}$; was calculated, where τ is the correlation time. The data was collected for a period of

10 second intervals and averaged over ten runs to get the autocorrelation function and the corresponding fits. All FCS data is an average of more than 20 sets. The pin-hole size was kept at 70 μm for 488 nm laser line (confocal diameter of ~ 300 nm) and 78 μm for 543 nm laser line (confocal diameter of ~ 360 nm). In our experiments, appropriate laser power of 488nm line (Argon-Ion laser – Lassos) was used to avoid artefacts arising due to photobleaching and to ensure high counts/particle.

The following functions were used to fit the experimentally obtained autocorrelation curves. For unhindered three-dimensional diffusion

$$G(\tau)=\left(\frac{1-A+A\cdot\exp(-\tau/C)}{1-A}\right)\left(\left(\frac{1}{N}\right)\left[\frac{1}{\left[1+\left(\frac{\tau}{\tau_D}\right)\right].\left[1+\left(1/s^2\right)\left(\frac{\tau}{\tau_D}\right)\right]^{1/2}}\right]\right) \qquad \ldots(1)$$

Here N is the number concentration of the fluorescent species in the confocal volume, τ_D is the diffusion timescale, such that diffusion constant $D=\omega^2/4\tau_D$, where ω is the XY spread of the confocal spot, and s is the structure parameter; A and C are the triplet fraction and triplet timescales respectively. However, for molecules like TMR-dextrans, activated notch, or the histone core particles, diffusion inside the cell nucleus cannot be adequately described by this model. In order to understand these results, I have used the modified autocorrelation function with an anomalous sub-diffusion term β, which is a useful parameter to describe the underlying heterogeneity of the matrix (26,[14, 15].

$$G(\tau)=\left(\frac{1-A+A\cdot\exp(-\tau/C)}{1-A}\right)\left(\left(\frac{1}{N}\right)\left[\frac{1}{\left[1+\left(\frac{\tau}{\tau_D}\right)^{\beta}\right].\left[1+\left(\frac{\tau}{s^2\tau_D}\right)^{\beta}\right]^{1/2}}\right]\right) \qquad \ldots\ldots\ldots \quad (2)$$

The data obtained for the linker histone dynamics was fitted to a sum of two diffusing species. For this, we used the maximum entropy method – MEMFCS (35), used in FCS experiments, to fit our data to independently verify our assumption of using sum of two diffusing species to describe the dynamics of linker histones.

$$G(\tau)=\left(\frac{1-A+A\cdot\exp(-\tau/C)}{1-A}\right)\left(\left(\left(N_1\cdot N_2\right)\left[\frac{1}{\left[1+\left(\frac{\tau}{\tau_{D_1}}\right)\right]\cdot\left[1+(1/s^2)\left(\frac{\tau}{\tau_{D_1}}\right)\right]^{1/2}}\right]\right)+\left(\left(N_1\cdot(1-N_2)\right)\left[\frac{1}{\left[1+\left(\frac{\tau}{\tau_{D_2}}\right)\right]\cdot\left[1+(1/s^2)\left(\frac{\tau}{\tau_{D_2}}\right)\right]^{1/2}}\right]\right)\right)$$

where, N_1 is the inverse of the total number of bright molecules (EGFP tagged linker histones) in the confocal volume and N_2 corresponds to the fraction of the species having correlation timescale τ_{D1}.

Figure 2.2.1

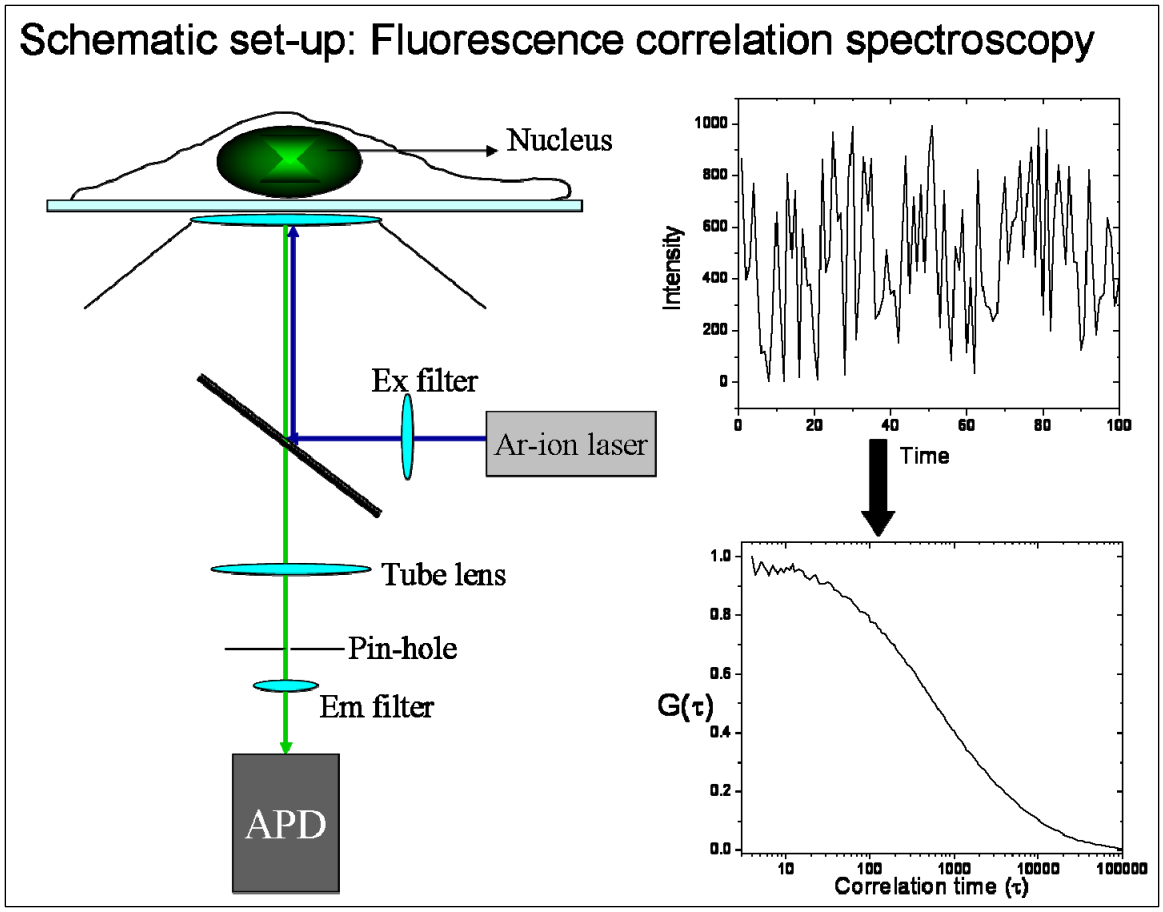
Schematic set-up: Fluorescence correlation spectroscopy
Nucleus
Ex filter
Ar-ion laser
Tube lens
Pin-hole
Em filter
APD
Intensity
Time
G(τ)
Correlation time (τ)

2.3.2 Results

(i) Core histones exist in a multimeric state inside the cell nucleus

Diffusion of the core histone H2B-EGFP

Histone proteins condense the DNA into a highly organized chromatin assembly. We explored the diffusion of the free fraction of core histone proteins (H2B) to assess their state and the interaction with the chromatin assembly inside a live cell nucleus. The mobility of core histone H2B tagged with EGFP (H2B-EGFP) within the cell nucleus was measured using FCS and the associated correlation curves are shown in **Figure 2.3.2(a)**. The typical correlation timescale is τ_D = 830.5 ± 232 μsec (the corresponding diffusion constant D = 7.3 ± 1.9 μm^2/sec) under normal physiological conditions. The standard deviation in the timescales reflects the heterogeneity in the chromatin assembly. Interestingly, the mean correlation timescale for H2B-EGFP is much higher than what is expected from its molecular size (~ 41 kDa, total), suggesting that it exists in a multimeric state. In order to test this, we measured the correlation timescale of H2B-EGFP in the cytoplasm, in transiently transfected HeLa cells over-expressing H2B-EGFP. The correlation timescale of H2B-EGFP in the cytoplasm τ_D = 268 ± 65.2 μsec (with β = 0.67) and the corresponding diffusion constant D = 22.2 ± 5.4 μm^2/sec were indicative of a monomeric state. It is likely that after the core histones translocate to the nucleus they multimerize.

Diffusion of the core histone H4-EGFP

We show here that one of the core histones H4-EGFP has similar diffusion characteristics like H2B-EGFP. From the autocorrelation curve we find that H4-EGFP also shows a sub-diffusive behaviour inside the cell nucleus in normal physiological condition, like the H2B-EGFP. H4-EGFP shows a mean correlation timescale ~871 ± 272 μsec (with β=0.67) with a corresponding diffusion constant of D = 7.3 ± 3.0 μm^2/sec.

In-vitro reconstitution experiments of the DNA-histone complex suggests that the association of different monomers of core histones do not happen simultaneously. Two dimeric H3-H4 complexes associate with the nascent DNA and form a tetrameric H3-H4-complex and the two another dimers of H2A-H2B interact with the complex and form the nucleosomal core particle.

(ii). Core histone mobility is conserved between mammalian and polytene cells

In order to test whether the core histone mobility is a generic feature, we measured H2B mobility in the polytene chromosomes of salivary glands derived from transgenic H2B-EGFP *Drosophila* fly [11]. In this system as well, H2B undergoes hindered diffusion with $\beta \sim 0.67$. Here, two distinct regimes in the distribution of correlation timescales $\tau_1 = 368 \pm 68$ μsec & $\tau_2 = 863 \pm 217$ μsec with the associated diffusion constants $D_1 = 15.8 \pm 3.2$ μm^2/sec & $D_2 = 6.8 \pm 1.3$ μm^2/sec were observed (Fig 2.3.2 (b)). The magnitude of these timescales is consistent with those observed in HeLa cells. Thus τ_1 represents the monomeric fraction of H2B-EGFP while τ_2 represents the multimeric H2B-EGFP. The larger presence of monomeric fraction of core histones in the polytene system, in comparison to HeLa cell nucleus, is perhaps due to the nature of chromatin organization in *Drosophila* salivary gland cells.

Figure 2.3.2(a)

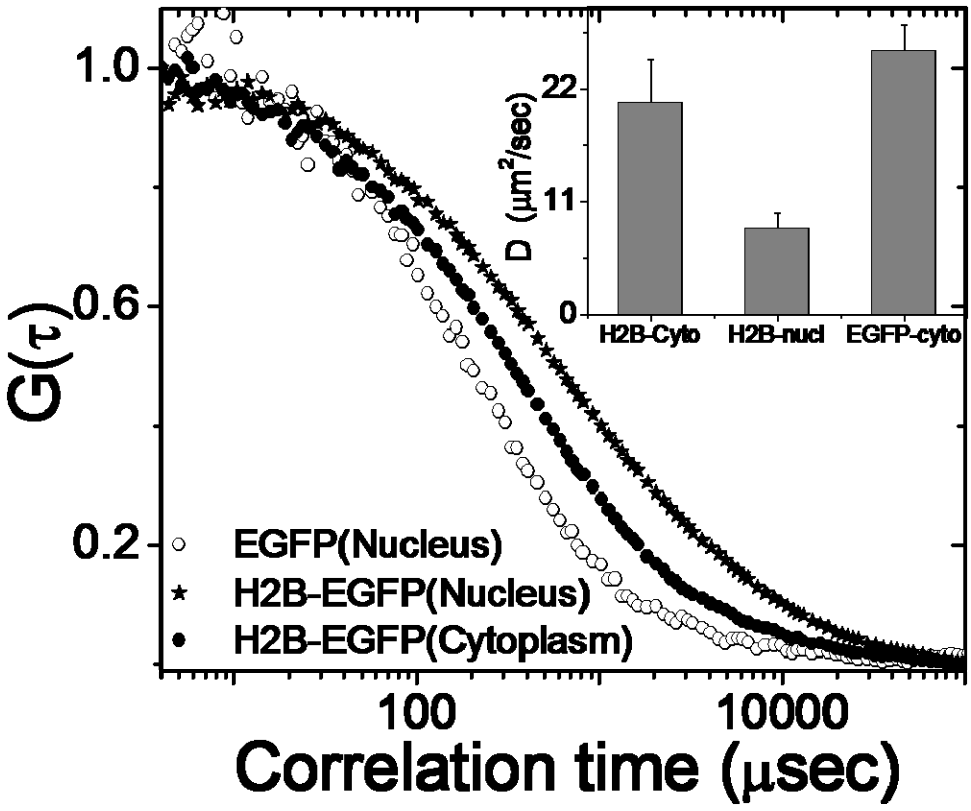

Core histone (H2B-EGFP) dynamics suggests their multimeric state. Autocorrelation curves of EGFP in the cell nucleus and H2BEGFP in the cytoplasm and in the nucleus. (Inset) Mean diffusion constants for the above cases.

Figure 2.3.2(b).

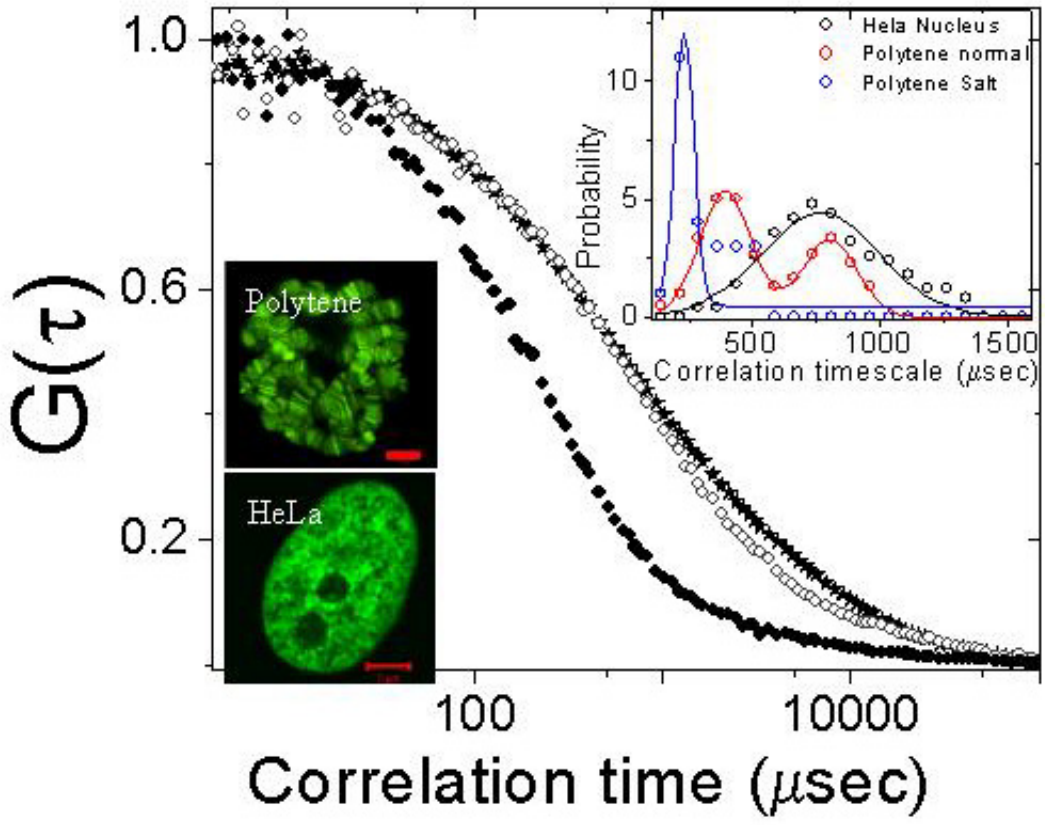

Histone mobility is conserved between mammalian and polytene cells. Fluorescence images of the *Drosophila* salivary gland cell nucleus (polytene chromosomes) and HeLa nucleus and the associated autocorrelation curves of H2B-EGFP proteins in HeLa nucleus (◊), salivary gland cell nucleus (*), and salivary gland cell nucleus with 600 mM NaCl (♦). (Inset) Probability histograms of the diffusion correlation timescales for H2B-EGFP in HeLa nucleus and salivary gland cell nucleus and comparison of the probability histograms with H2B-EGFP diffusion in salivary gland cells in 600 mM NaCl concentration.

(iii). Spatial heterogeneity of chromatin architecture determines core histone mobility

The heterogeneity of the chromatin structure was altered using salt-induced disassembly of nucleosomes. Upon addition of 600 mM NaCl [12], the chromatin architecture is affected which is reflected in the change of β value. Here the correlation curve fits perfectly with single species normal 3D unhindered diffusion with a single mean correlation time scale of 301 ± 104 μsec with the corresponding D = 20.9 ± 6.9 μm^2/sec **(Fig2.3.2(c))**. The lower correlation time of H2B-EGFP upon addition of 600 mM NaCl is possibly due to the dissociation of both free and bound multimeric H2B-EGFP into monomers. With the addition of salt, the change in β value from 0.67 to 1 and the decrease in the standard deviation of correlation timescales suggest that diffusion of core histone proteins is dependent on the spatial heterogeneity of chromatin architecture within the cell nucleus.

(iv). Estimation of monomeric Histone (H2B-EGFP) diffusion timescale in HeLa nucleus.

The experiments described below detail the estimates of the expected monomeric diffusion timescale of the H2B-EGFP inside the HeLa cell nucleus.

Comparing EGFP diffusion inside the cell nucleus and in PBS solution

Fluorescence Correlation Spectroscopy has been used to measure EGFP diffusion inside cell nucleus and in the PBS solution. EGFP molecules diffuse through the confocal volume, in ~80μsec (τ_{D2}) and ~220 μsec (τ_{D1}) in PBS solution and when expressed in HeLa cells, respectively. Assuming the structure of EGFP is not changed significantly inside the cell nucleus, one can estimate the ratio of the η values in the nucleus (η_1) and in PBS solution (η_2).

$$\frac{\tau_{D_1}}{\tau_{D_2}} = \frac{D_2}{D_1} = \left(\frac{\eta_1.a_1}{\eta_2.a_2}\right) = \frac{220}{80} = 2.75$$

when, $a_1=a_2$

Comparing, I get the ratio $\left(\frac{\eta_1}{\eta_2}\right) = 2.75$; the ratio of the viscosities inside the cell nucleus and in PBS buffer for EGFP molecules.

(a) Comparing H2B-EGFP diffusion inside the cell nucleus and in PBS solution

To estimate the typical diffusion timescale of H2B-EGFP monomers in PBS solution, we purified mono-nucleosomes from HeLa nuclei using standard protocols. 600 mM NaCl buffer was added to the sample to ensure that H2B-EGFP dissociates to its monomeric form. The sample was centrifuged at 5000 rpm for 5 min. to remove all the debri and the supernatant was used in FCS experiments. From the autocorrelation curve, we can get the typical correlation timescale of the monomeric H2B-EGFP ~120 μsec (τ_{D2}). Using $\left(\frac{\eta_1}{\eta_2}\right) = 2.75$ as the ratio of the viscosities inside the cell nucleus and in PBS buffer, one can estimate the typical correlation timescale (τ_{D1}) for monomeric H2B-EGFP inside the cell nucleus.

$$\tau_{D_1} = \tau_{D_2}.\left(\frac{D_2}{D_1}\right) = \tau_{D_2}.\left(\frac{\eta_1.a_1}{\eta_2.a_2}\right) = \left(120\mu s \times 2.75\right) = 330\,\mu s.$$

When, $a_1=a_2$,

We get the expected value of the monomeric H2B-EGFP correlation timescale as ~330 μsec. This value is similar to the mean correlation timescale obtained from our experiments obtained in the cytoplasm.

The correlation timescale of H2B-EGFP in the cytoplasm τ_D = 268 ±65.2 µsec, indicates the core histone (H2B-EGFP) remains in the monomeric form in the cytoplasm of HeLa cells, but in the cell nucleus H2B-EGFP remains in the multimeric form, as the viscosities in the cell cytoplasm and inside the nucleus for EGFP molecules are similar. Instead of heterogeneity in the cell nucleus, we think it is a multimeric form of H2B-EGFP which gives rise to a correlation timescale ~τ_D= (830.5±232) µsec.

Figure 2.3.2(C)

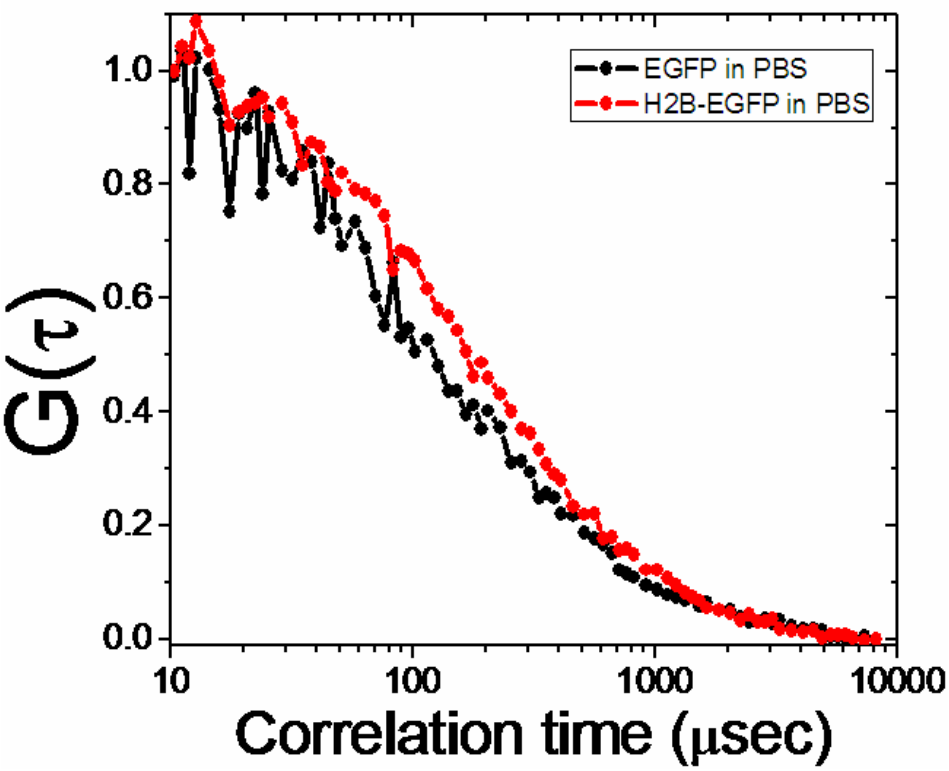

Probing core histone monomers in PBS solution. Representative autocorrelation function curves for EGFP molecules (Black) and H2B-EGFP molecules (Red) in PBS solution.

(v). Linker histones have a distinct interaction timescale

Linker histone diffusion is distinct from core histones and reveals two timescales

Linker histones bind at the entry and exit sites of DNA on the nucleosome to form a stable higher order chromatin structure and this interaction has been suggested to be highly dynamic **[16, 17]**. From FRAP measurements of the linker histones we can find that the recovery of linker histones is significantly different from the core histones (H2B-EGFP/ H4-EGFP) as well as free EGFP expressed inside the HeLa cell nucleus. For a non-interacting protein like EGFP recovery is significantly faster (∠2sec) than the linker histones indicating a purely diffusive fluorescence recovery, whereas core histones do not show any significant indication of dynamic exchange between the bound and free ones. Linker histone recovery (~ 100s of sec, depending upon the bleached area and differ subtypes of linker histones) is indicative of large exchange between the bound and free ones. So in this context it is important to understand the diffusive mechanism of the linker histones inside the live cell nucleus in normal physiological conditions.

FCS data show that the autocorrelation behaviour of the linker histone protein H1.1-EGFP is significantly different from that of the core histone proteins **Figure 2.3.2(d)**. Here the FCS curves do not fit with single species 3D unhindered diffusion or with the anomalous diffusion. Clearly there is a second distinct timescale in the autocorrelation function, which may be attributed to the dynamic interactions of the linker histones with the chromatin fibre. To obtain the underlying diffusion timescales, we have fitted the data with a two species diffusion model described in the methods section. The fits to the data show two distinct timescales (τ_{D1} = 298.3 ± 58.8 μs) with diffusion constant D_1 = 19.5 ± 3.5 μm^2/sec commensurate with 3D diffusion, and (τ_{D2} = 26.5 ± 12.8 ms) D_2 = 0.3 ± 0.1 μm^2/sec possibly arising due to H1.1-EGFP interaction with DNA.

Tail residues determine the interaction timescales of linker histone diffusion

In order to gain more insight into the origin of the second time scale (τ_2), the amino acid residues (1 to 40 and 121 to 216) corresponding to the N and C terminal tail sequences of H1.1 were deleted. Deleting the tail residues of H1.1-EGFP histones abolished the second diffusion time scale and the resultant FCS curves (**Figure 2.3.2(d))** fit well with single species unhindered 3D diffusion with $D = 20.2 \pm 5.2\ \mu m^2/sec$. H1.1 tails could both interact with DNA as well as with adjacent histones on the chromatin assembly suggesting that these interactions are the source of the second timescale (τ_2) [18]. FRAP experiments presented in inset to **Figure 2.3.2(d)** for H1.1-EGFP, tail-less H1.1-EGFP in comparison with free EGFP, H4-EGFP and H2B-EGFP strongly support our conclusions. In order to test the origin of the second timescale (τ_2) of the linker histones, we measured the correlation timescale of strongly interacting H1.5-EGFP in the cytoplasm in transiently transfected cells over-expressing H1.5-EGFP. FCS curves showed a single species sub-diffusive autocorrelation behaviour with mean correlation timescale $376.6 \pm 132.4\ \mu sec$ (with $<\beta> = 0.72$ reflecting the cytoplasmic anomalous diffusion factor). This indicates that the second time scale (τ_2) of the linker histones within the nucleus arises primarily due to its interaction with the chromatin assembly.

Figure 2.3.2(d)

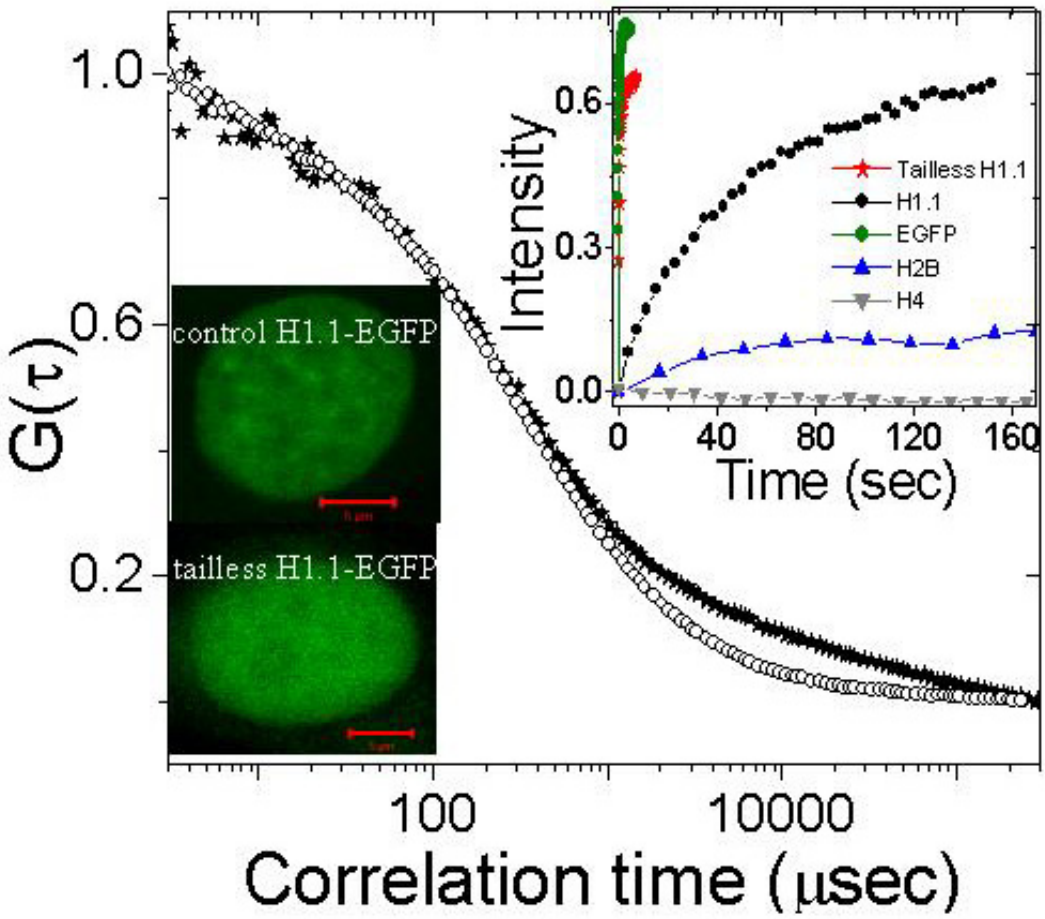

Linker histone shows distinct interaction timescales inside the cell nucleus. Fluorescence images of H1.1-EGFP and tailless H1.1-EGFP transfected HeLa nucleus (scale bar, 5 μm) and the associated autocorrelation function curves for H1.1-EGFP (*), tail-less H1.1-EGFP (O). (Inset) Fluorescence recovery curves for tail-less H1.1-EGFP, H1.1-EGFP, EGFP, and core histones, H2B-EGFP and H4-EGFP.

Figure 2.3.2(e)

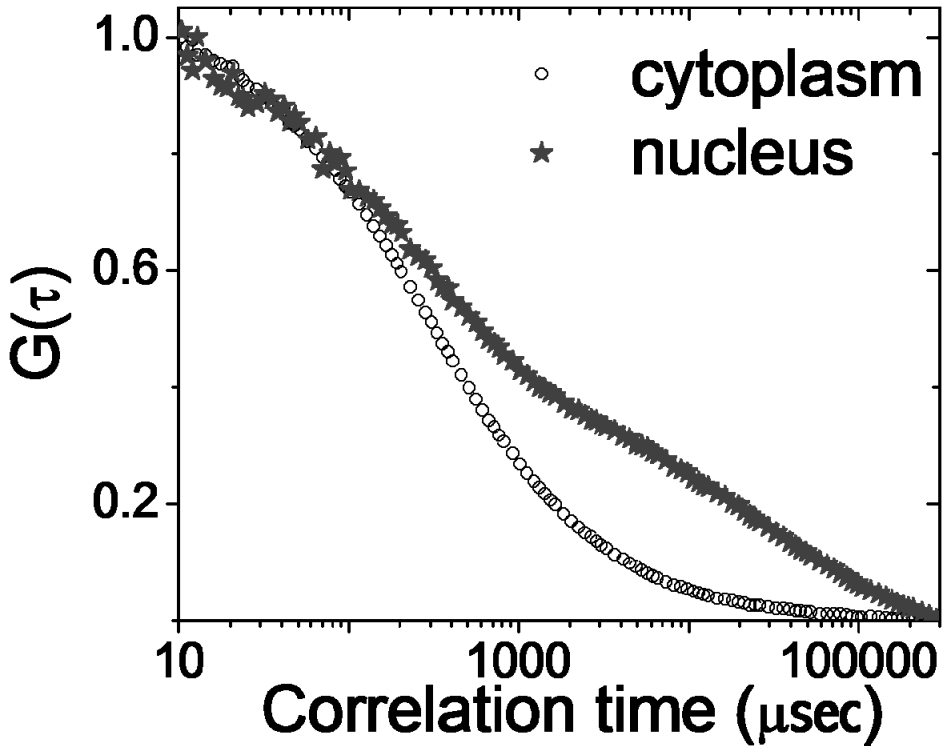

Autocorrelation function curves for H1.5-EGFP, in the cytoplasm and inside the cell nucleus.

(vi). Linker histone subtypes show distinct changes in their mobility.

The diffusion characteristics of the various linker histone subtypes (H1.2, H1.4 and H1.5) were also studied using FCS. These histones also showed two distinct timescales of diffusion where the mean second timescale (τ_2) corresponded to 28 msec, 34 msec, 34 msec for H1.2, H1.4, H1.5 respectively (**Figure- 2.3.2(f) and, 2.3.2(g)**). A fit of the interaction timescale (τ_2) with a normal distribution shows that the peak values of the distribution function is statistically distinct for H1.1, and H1.2 compared to H1.4 and H1.5 (**Figure 2.3.2(g)**). The C terminal tails of H1.1 and H1.2 are smaller, with less number of interacting residues, than that of H1.4 and H1.5. This is possibly reflected in the shorter diffusion timescale commensurate with their tail lengths that define the extent of interactions. The data on the fraction of interacting linker histone subtypes is shown in inset to **Figure 2.3.2(g)**.

To probe the differences in mobility between different linker histone subtypes, both FRAP and FCS experiments were performed within the live cell nucleus. In FRAP experiments, the bleaching cross-section was ~ 3 μm and the mean recovery curve was an average of the FRAP from 10 different cells. The FRAP data shows that the fluorescence recovery of the linker histones are markedly faster than the core particles (H2B and H4). This is in line with previous observations in the literature **[16, 17]** and is characteristic of the dynamic nature of interactions associated with linker histones. A comparison of the FRAP data between different subtypes of H1 proteins shows that the H1.1, H1.2, H1.4, H1.5 recover to about 96%, 87%, 83%, 83% in a time duration of 160 seconds. In contrast, core histones H2B and H4 recover to < 20% over a 30 min timescale.

Figure 2.3.2(f)

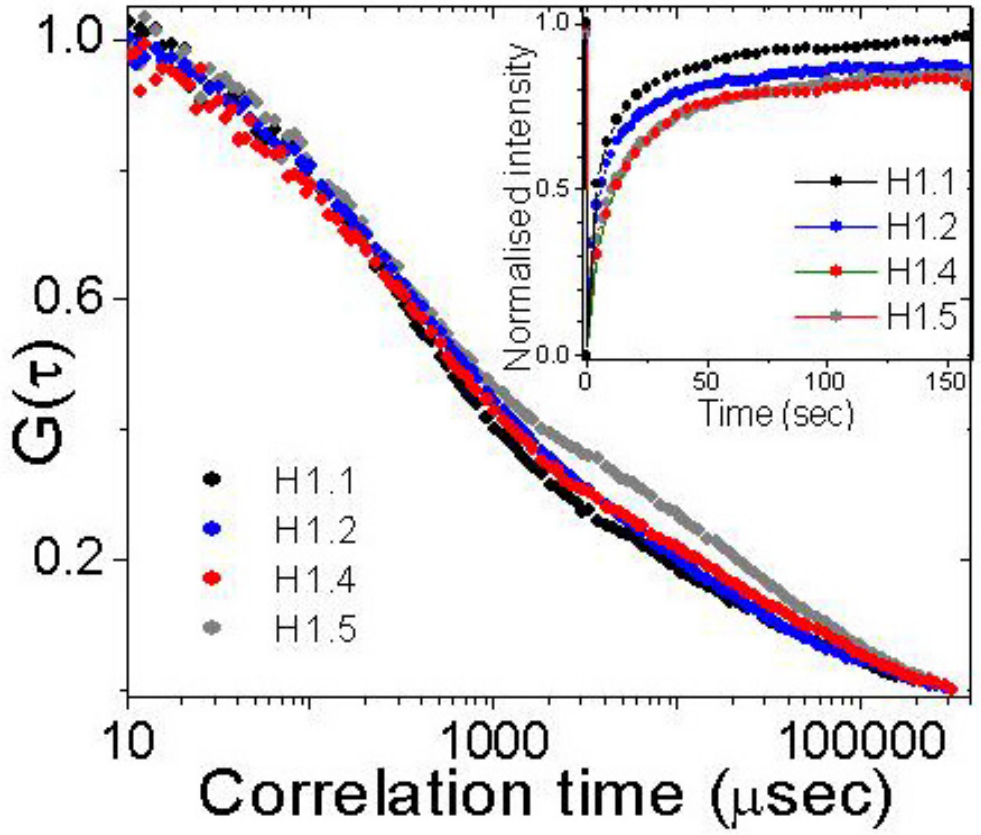

Different subtypes of H1 proteins show distinct interaction timescales. Autocorrelation curves for different H1 subtypes, H1.1, H1.2, H1.4, and H1.5, inside the HeLa cell nucleus. (Inset) Normalized FRAP data for different subtypes of H1 proteins, H1.1, H1.2, H1.4, and H1.5.

Figure 2.3.2(g)

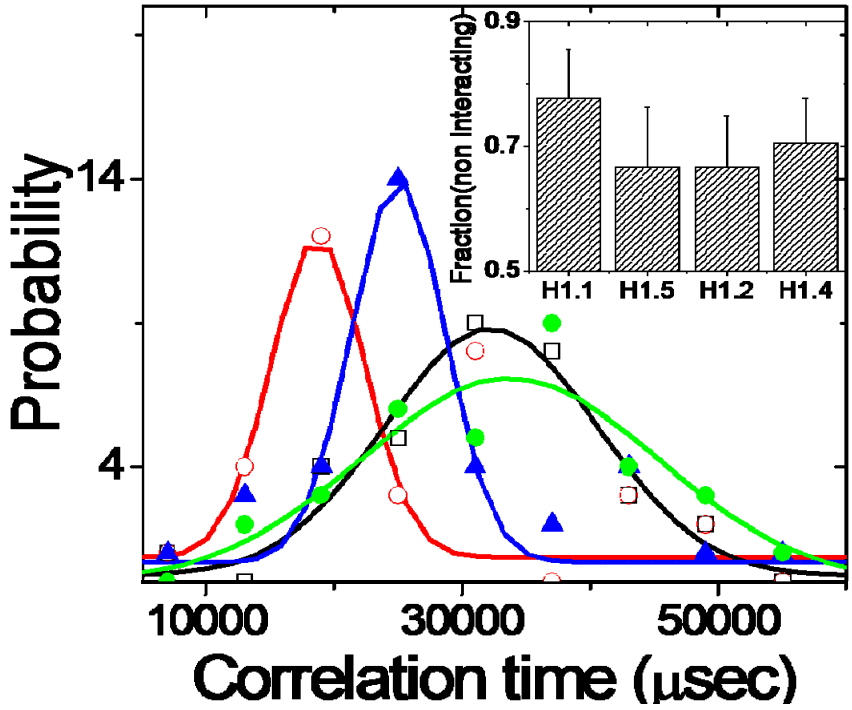

Probability histograms of the interaction timescale of different subtypes of H1 proteins H1.1-EGFP (Red), H1.2-EGFP (Blue), H1.4-EGFP (Green), H1.5-EGFP (Black). Inset - Mean and standard deviations of the fractions of the non-interacting species in different H1 subtypes

(vii). Alterations in core and linker histone diffusion during ATP depletion.

(a).The multimeric form of the core histones is ATP dependent

Our experiments have shown that the freely diffusing core histones (H2B-EGFP and H4-EGFP) are in a multimeric form inside the cell nucleus in normal physiological condition, though in the cytoplasm of an over-expressed cell they stay in the monomeric form. From literature, we know the incorporation of core histones in the chromatin fiber is ATP dependent in live cell nucleus **[19]**. ATP dependent chaperons are involved in the incorporation of the core histones. So, it is important to understand the role of ATP in maintenance of the multimeric form of the freely diffusing core histones in live cell nucleus.

In order to probe whether the multimeric state of the H2B is ATP dependent, FCS measurements were done on H2B-EGFP in ATP depleted HeLa cells. **Figure 2.3.2(h-(i))** shows the distribution of correlation timescales of H2B-EGFP diffusion in HeLa cell nucleus under normal and ATP depleted conditions. Upon ATP depletion, there is a significant decrease in both the mean correlation time scale τ_D = 533.5 ± 248.3 μsec (D = 12.7 ± 5.3 μm^2/sec). The distribution of correlation timescales in different ATP depleted cells indicate the emergence of a fast timescale significantly similar to the timescale estimated for monomeric H2B-EGFP diffusion (~330 μsec) in HeLa nucleus. We have seen from the diffusion measurement of passive particle (EGFP and TMR-dextrans) upon ATP depletion the viscosity (η) of the cell nucleus and the chromosomal mesh structure (β value) do not change significantly. We expect this lowering in diffusion time scale of H2B-EGFP is due to an enriched monomeric fraction upon ATP depletion, suggesting that the maintenance of the multimeric state is an energy dependent process.

Figure 2.3.2 (h-(i))

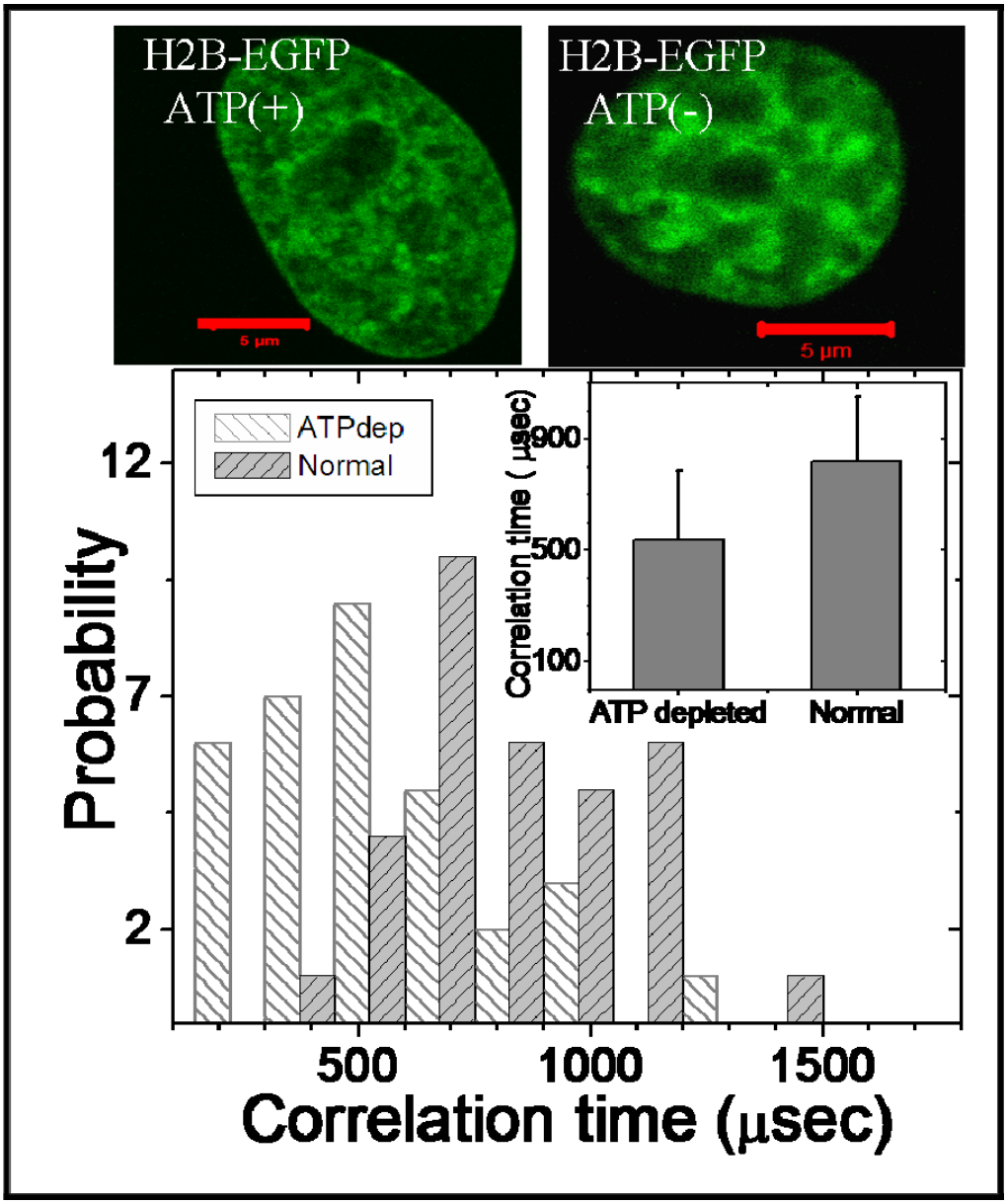

Fluorescence images of H2B-EGFP transfected HeLa nucleus before and after ATP depletion (Scale bar, 5 μm). Probability histograms of correlation timescales of H2B-EGFP diffusion inside HeLa nucleus before and after ATP depletion. Inset: The bar graphs of the mean correlation timescales

(b). Interaction timescales of the linker histones are independent of ATP content in the cell

Our earlier studies reveal that the diffusion of linker histones is influenced by their transient binding and unbinding with the chromatin fibre. FCS experiments have been used to estimate the typical interaction timescales of different subtypes of linker histones with the chromatin fibre. It therefore becomes important to understand the possible involvement of active mechanisms in the interaction of the linker histones with the chromatin fibre.

FCS measurements of linker histones were carried out on ATP depleted HeLa cell nucleus. Fluorescence autocorrelation curves of H1.5-EGFP transfected cells in ATP depleted condition show the existence of interaction timescales. Plotting the distribution of the interaction timescales of H1.5-EGFP under ATP depleted condition and comparing the timescale distribution of the same under normal physiological condition, I have observed that the interaction timescale of linker histones (H1.5-EGFP) is ATP independent as shown in **figure 2.3.2(h-(ii)).**

Figure 2.3.2(h-(ii))

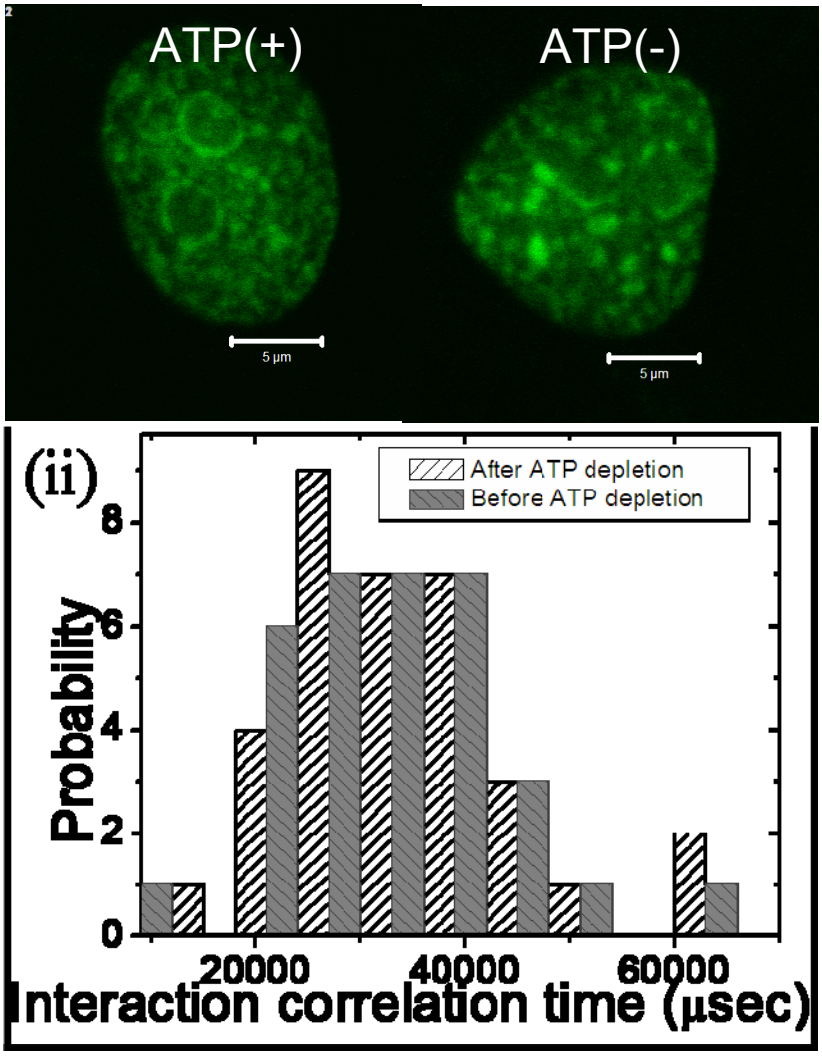

Fluorescence images of H1.5-EGFP transfected HeLa nucleus before and after ATP depletion (Scale bar, 5 μm). Probability histograms of H1.5-EGFP correlation timescale in milliseconds, before and after ATP depletion.

(viii). Alterations in core and linker histone diffusion during cell death

Histone dynamics also depends upon the state of the cell. As histone proteins are one of the major factors of maintenance of nuclear structure and function. In this context it is important to understand the change in histone dynamics with cell death. To elucidate the effect of large-scale changes in the chromatin structure on diffusive behaviour of histones, we performed FCS experiments on apoptotic HeLa cells where apoptosis was induced by addition of 10 μM staurosporine. Integral chromatin proteins, like H2B-EGFP and H4-EGFP, showed complete loss of correlation signal under these conditions (**Figure 2.3.2(j)**. However, less tightly associated proteins like the linker histones (H1.1) and non interacting proteins such as EGFP, showed only a partial loss of correlation in FCS experiments. This indicates that the free fraction of the core histones (H2B-EGFP or H4-EGFP) becomes highly immobile, possibly as a result of chromatin condensation characteristic of the apoptotic state. In this case, the diffusion constant could not be extracted for the core histones, as there was a total loss of correlation signal on induction of apoptosis. Fluorescence imaging shows that the inherent fluorescence intensity levels do not change significantly upon treatment with staurosporine, indicating minimal leakage of the free core histones from the nucleus under these conditions. The fluorescence confocal image **(Inset to Figure 2.3.2(j)–(i))** shows punctated bright structures upon induction of apoptosis, indicating the heterogeneity in chromatin compaction. Further to elucidate changes in linker histone mobility in apoptotic cells, FRAP experiments were carried out on HeLa cells expressing strongly interacting H1.5-EGFP under normal and apoptotic conditions. FRAP recovery is significantly slower under conditions of apoptosis relative to normal cells **(Figure 2.3.2(j)-(ii))**.

These findings using a combination of FCS and FRAP techniques on both linker and core histones, suggest that the diffusion of core histones, is more

adversely affected by induction of apoptosis in comparison with those of linker histones or a free molecule that interact less with the chromatin.

Figure 2.3.2(j)

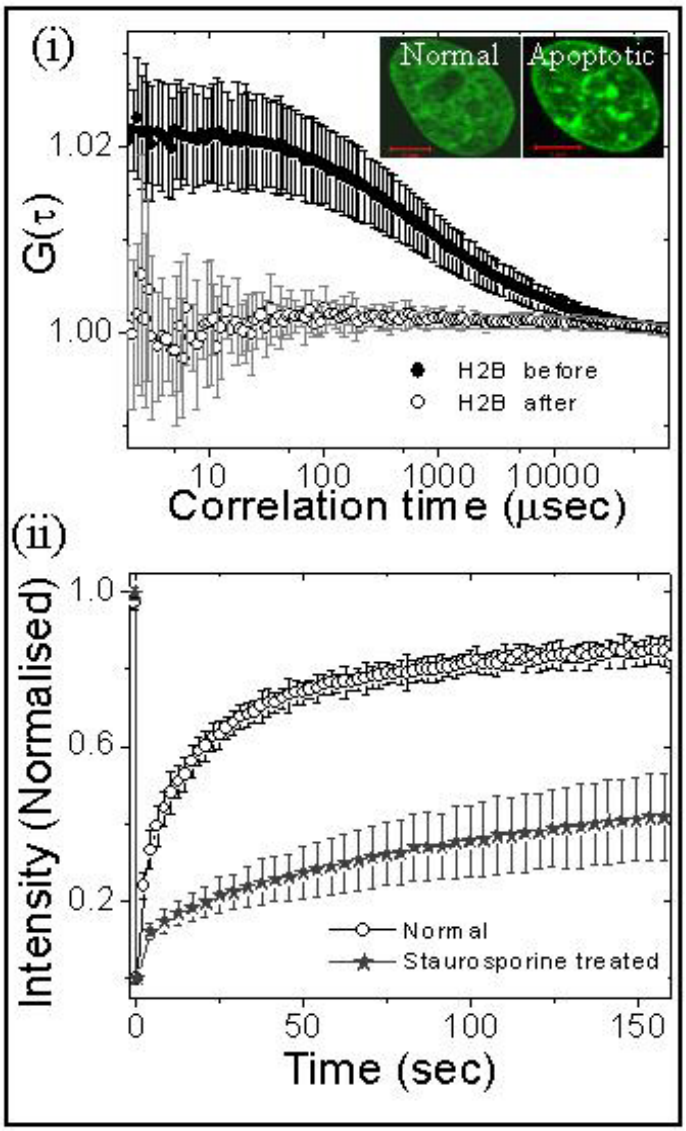

Time course of histone protein dynamics within cells upon induction of apoptosis. (i) Autocorrelation function curves for H2B-EGFP before and after 4 hours of addition of staurosporine in HeLa cells. (Inset) Fluorescence images of H2B-EGFP transfected HeLa cells before and after addition of staurosporine. (Scale bar, 5 μm). (ii) FRAP curves for H1.1-EGFP in HeLa cells, in normal conditions and after staurosporine treatment.

(ix). Colocalization between different subtypes of linker histones.

It is known that the percentage of different subtypes of linker histones vary significantly between different cell types **[20]**. Thus it becomes important to understand the functional localization of different linker histones in a cellular context. We have used multicolor confocal fluorescence imaging as a comparative measure of the localization of different linker histone subtypes.

H1.4 tagged to mRFP is transiently transfected on to a stable H2B-EGFP cell line. Colocalization experiments indicate that the linker histone H1.4-EGFP strongly colocalises with the core histones in the inter-phase cells. The co-localization of different subtypes of linker histones in interphase HeLa cells has also been studied. Transient transfections of H1.4-mRFP in stably or transiently transfected H1.1-EGFP, H1.2-EGFP or H1.5-EGFP cell lines was done. In the interphase HeLa cells, a partial co-localization between different sub-types of linker histones has been observed. In control cells, a complete co-localization between H1.4-EGFP and H1.4-mRFP is observed. This indicates that the partial colocalization between different subtypes of linker histones is not an artifact of the fluorescence tagging.

Figure 2.3.2(k)

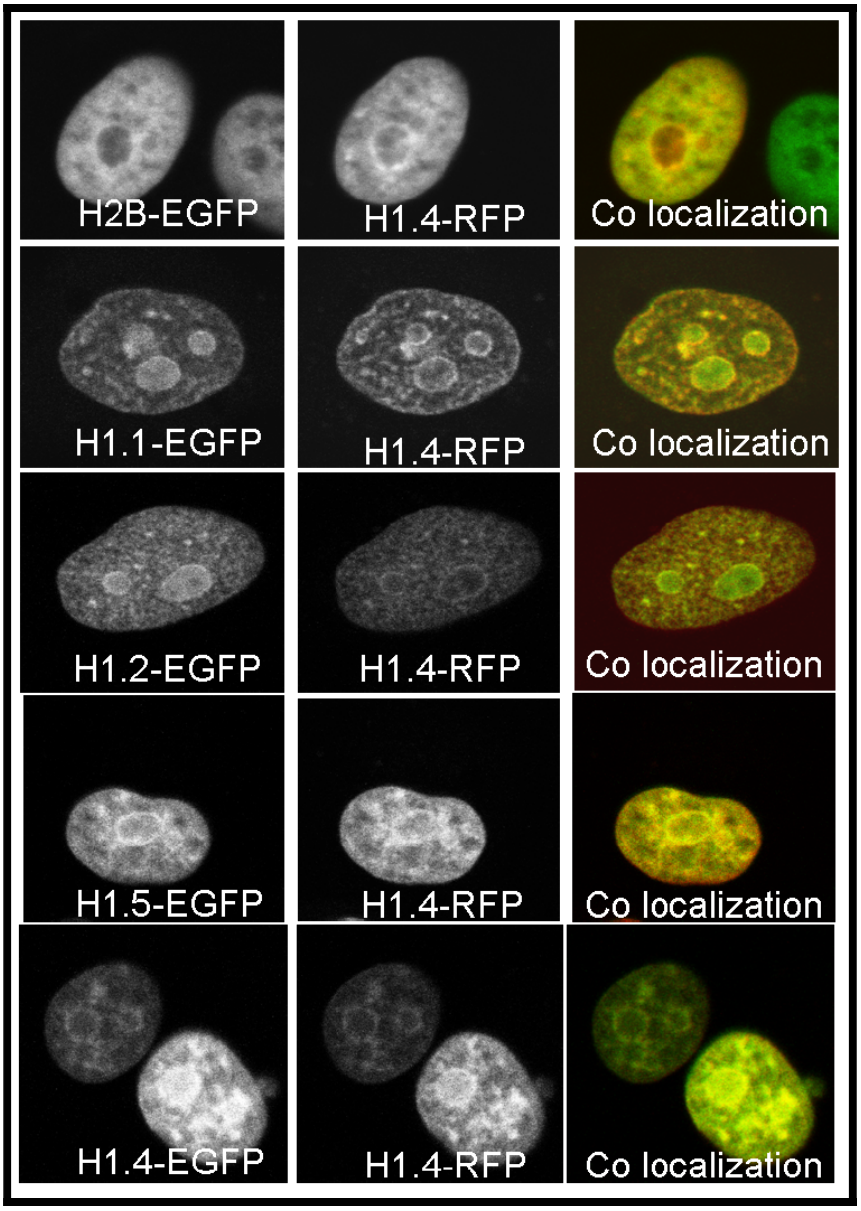

Colocalization of different linker histones inside the HeLa nucleus.

(i) Colocalisation of H1.4-mRFP with H2B-EGFP in the HeLa nucleus.
(ii)Colocalisation of H1.4-mRFP with H1.1-EGFP in the HeLa nucleus.
(iii) Colocalisation of H1.4-RFP with H1.2-EGFP in the HeLa nucleus.
(iv) Colocalisation of H1.4-RFP with H1.5-EGFP in the HeLa nucleus.

2.4- Numerical simulations and a schematic model to understand the distinct diffusive behavior of the core and linker histones

In the cellular environment, the motion of a particle is governed by diffusion through constrained geometry and its interaction with other organelles. The diffusion of a protein in a molecular crowded environment and its interaction with other particle influence the functionality of different protein complexes. In a homogeneous solution the diffusive motion of a spherical object follows Einstein's equation. Where mean square displacement $\langle \Delta X \rangle^2$ of a particle after a certain time (t) follows Stoke-Einstein relation $\langle \Delta X \rangle^2 = 2 \cdot n.D.t$, where, n corresponds to the number of degrees of freedom. From Stoke-Einstein relation we find the normal diffusion of a particle is governed by thermal force (k_BT) and viscous drag giving rise to the diffusion coefficient $D = \frac{k_B T}{6\Pi \eta a}$; where, η is the viscosity of the medium (for water η= 1 cPoise for water at 20^0 C) and 'a' corresponds to the radius of the spherical diffusive object. The diffusion behavior of different histone monomers in a cell nucleus is complicated not only because of its higher nuclear concentration and a complex chromosomal mesh structure but also because of their probable interaction with the chromatin fiber. A numerical simulation has been done to understand the diffusion behavior of different histone monomers inside the cell nucleus.

2.4.1 Methods

Numerical simulation of Brownian Diffusion

LabView software of National Instruments has been used to simulate Brownian diffusion of particles. Here the particles undergo 3-D random walk with equal probability in each direction. A particle crossing the confocal volume, located around (0, 0, 0) position with a Gaussian profile,

$I(t) = I_0 \frac{1}{\sqrt{2\pi\sigma^2}} \exp\left[\frac{-\left(x^2+y^2+z^2\right)}{2\sigma^2}\right]$, contribute to the intensity (fluorescence) signal, depending upon its coordinate in the profile. The total intensity in each time trace for N such particles is then calculated. From the total intensity signal I(t), the autocorrelation function $G(\tau) = \frac{\langle I(t+\tau).I(t)\rangle - \langle I^2(t)\rangle}{\langle I^2(t)\rangle}$ is calculated and is averaged over a number of traces. The mean autocorrelation function is calculated by averaging over the autocorrelation function $G_i(\tau)$ from several time traces. We find that the averaged autocorrelation function of a smaller non-interacting particle, starting from any random site, in a homogeneus medium gives a single correlation timescale as expected while the diffusion of two species with different step sizes will give two distinct correlation timescales.

To understand the diffusion of larger particles through the complex chromosomal mesh structure a mesh network in 3D with fixed or variable mesh sizes has been simulated. As the particle diffuses through the mesh structure with a certain probability it reflects back or becomes partially trapped, depending upon its step size, mesh size and the probability of transmission through the mesh structure. So, effectively the particle has asymmetric step sizes in different directions. In this case, the particle diffusion does not follow normal 3-D diffusion equation $\langle \Delta X \rangle^2 = 2 \cdot n.D.t$. Here diffusion equation follows anomalous sub-diffusion, $\langle \Delta X \rangle^2 = 2 \cdot n.D.t^{\beta}$; where $\beta<1$. From the experimental results we find that macromolecules, like EGFP tagged core-histone complex [21] follows this kind of sub-diffusive transport, whereas non-interacting smaller particles, like EGFP molecules follow normal diffusion.

2.4.2 Results

(i). Single species normal diffusion in 3 D

Random steps of the particles in 3-dimension with equal probability in all directions are generated with fixed step size starting from any random site. The diffusion trajectory of a particle having 4000 random steps, starting from any random site with step sizes 0.4 units, in the confocal volume 25 units is also generated. The 2D projection of the diffusion trajectory of a 3D random walker as generated in our simulation is shown in the **Figure 2.4.1(a)**. The square of the average displacement varies linearly with time, indicating normal 3-D diffusion as shown in the **Figure 2.4.1(a)**-Inset. At the time of diffusion as the particle crosses the confocal volume depending upon its coordinate it contribute to the fluorescent signal. From the total intensity $I(t) = \sum_n I_n(t)$ contributed by N such particles in a time trace, the autocorrelation function $G(\tau) = \frac{\langle I(t+\tau).I(t) \rangle - \langle I^2(t) \rangle}{\langle I^2(t) \rangle}$ is calculated. The number of particles (N) in each time trace (100) is fixed in such a manner that there is effectively one particle in the confocal volume in each time trace. The averaged autocorrelation function for such a random walker is shown in the **Figure 2.4.1(b)** and it gives rise to a single diffusion timescale as expected.

(ii). 3D normal diffusion of two particles with different step sizes

To understand the diffusive behavior of two different particles with different step sizes, numerical simulations have been done and we have shown that the autocorrelation function curves generated in our numerical simulation can decipher the distinct timescales for different particles. The simulation has been attempted as a two species diffusion using the parameters obtained from our experiments. Here we have generated the diffusion trajectories of a mixture of two particles having 4000 random steps with step sizes 0.4 and 4 units, and the size of our confocal volume 25 units. Initially, these particles are distributed in different random sites

in 3-D in the 3D space with dimension 80 times the size of the confocal volume. The number of particles (100) in each time trace is fixed in such a manner that there is effectively one particle in the confocal volume in each time trace. These simulations confirm the presence of two distinct timescales in the autocorrelation curves. In **Figure 2.4.1(c)**, we have shown the averaged autocorrelation function (Averaged over 60 such iterations) for a mixture of two different species.

Figure 2.4.1(a)

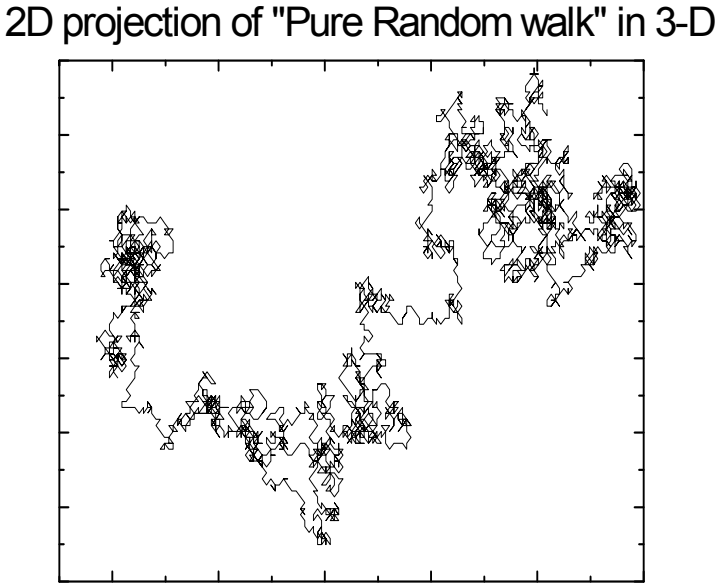

The 2D projection of a normal 3-D diffusion trajectory of a particle is shown in the figure.

Figure 2.4.1(b)

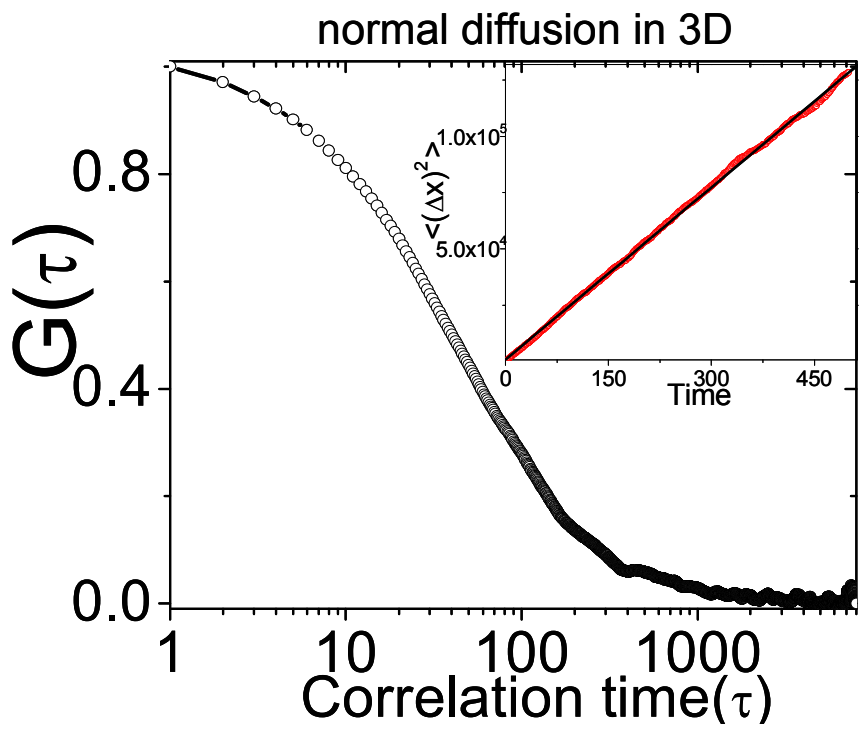

The autocorrelation function of a normal 3D diffusion. (Inset) The square of the displacement varies linearly with time for normal 3D diffusion.

Figure 2.4.1(c)

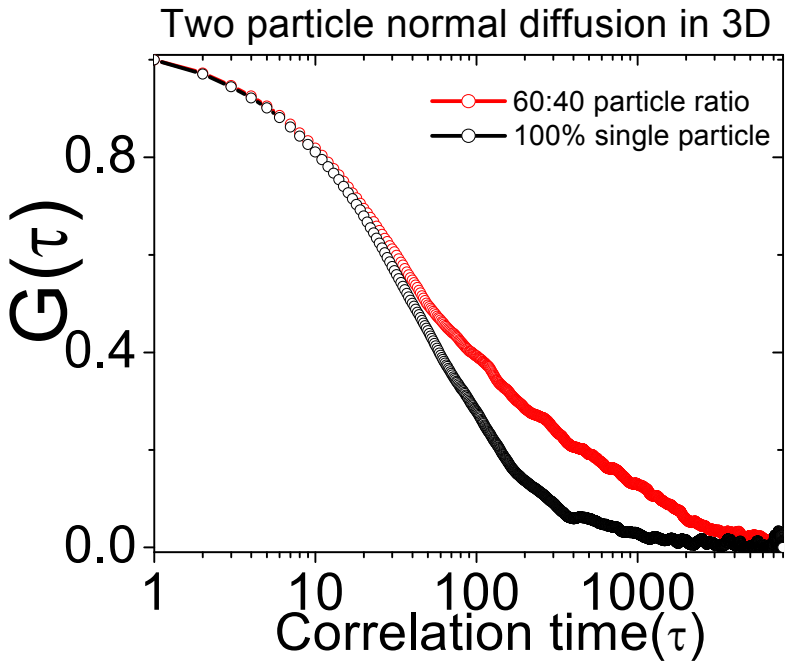

The averaged autocorrelation function (Averaged over 60 such iterations) for single species 3-D normal diffusion and for a mixture of two different species having step sizes 0.4 units and 4 units, respectively.

(iii). Diffusion through a mesh network (Origin of sub-diffusion)

FCS experiments show that the diffusion mechanism of core histones is different from the normal 3D diffusion shown by single species. To understand the origin of the sub-diffusive mobility of the core histones, a numerical simulation is done mimicking the experimental conditions.

Moving mesh network.

A 3-D homogenous mesh has been created with mesh size varying from 10, 15, 20, 50 units with 20% variability in the mesh size for each time step of the particle. As the particle enters the confocal volume, it gets excited and fluoresces. The total intensity of N such particles give the autocorrelation function. This autocorrelation function is compared to that of the particles diffusing in the absence of a complex, mesh structure.

Particles starting from any random site diffuse in 3D with step size 10 units through the mesh structure. As the particle tends to move to a site already occupied by a mesh, it reflects back and stays in its earlier position thereby introducing a time delay n its diffusion. The 'transmission probability' of a diffusing particle, is defined as the probability of crossing the mesh (1- probability of reflecting back).

Plots of the square of the displacement to time for an average of 100 particles of step length 10 units, diffusing through a mesh of size 11 (Red), 12 (Green), 15 (Blue) units, compared with the diffusion without mesh (Black) (**Figure 2.4.1(e)**, inset) show that this diffusion is distinctly different from normal diffusion ($<\Delta X^2> \propto t^{\beta}$, when $\beta<1$) with decrease in the mesh size. The diffusion trajectory of the particle also shows a compartmentalization effect depicted in the figure (**Figure 2.4.1(d)**).

From the simulation results it is clear that as the mesh size decreases, the particle confinement increases and sub-diffusive behavior overtakes indicated by a decrease in β factor. Comparing our experimental results with the simulation

study, we infer that as the size of a particle increases its diffusion tends to be more confined within the local chromosomal mesh, giving rise to sub-diffusive characteristics. In the simulation study when the particle step size (10 unit) and the mesh size (11unit) are kept constant, with only the probability of crossing the mesh varying from 5 % to 50%, we found that the diffusion process becomes purely diffusive and β approaches 1. Our simulation results confirm our experimental findings of sub diffusive mobility of the core histones within the cell nucleus though the freely moving EGFP molecules show normal 3D diffusion.

Figure 2.4.1(d (i))

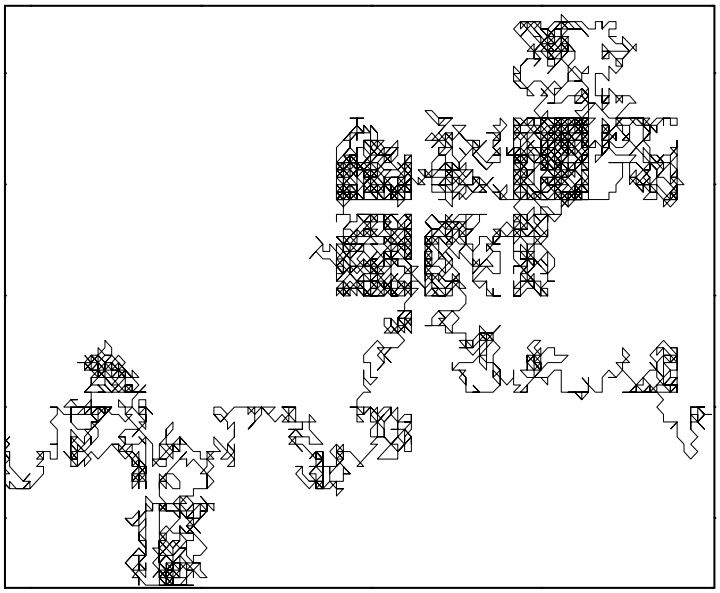

2-D projection of a 3-D random walk of a particle diffusing through a mesh structure with 20% variability. The diffusion becomes sub-diffusive as the particle diffuses through a mesh like structure. With increase in mesh structure the particle motion approaches normal diffusion. The increase in β (0> β >1) towards unity is a reflection of the transition from sub-diffusion to normal diffusion.

Figure 2.4.1(d(ii))

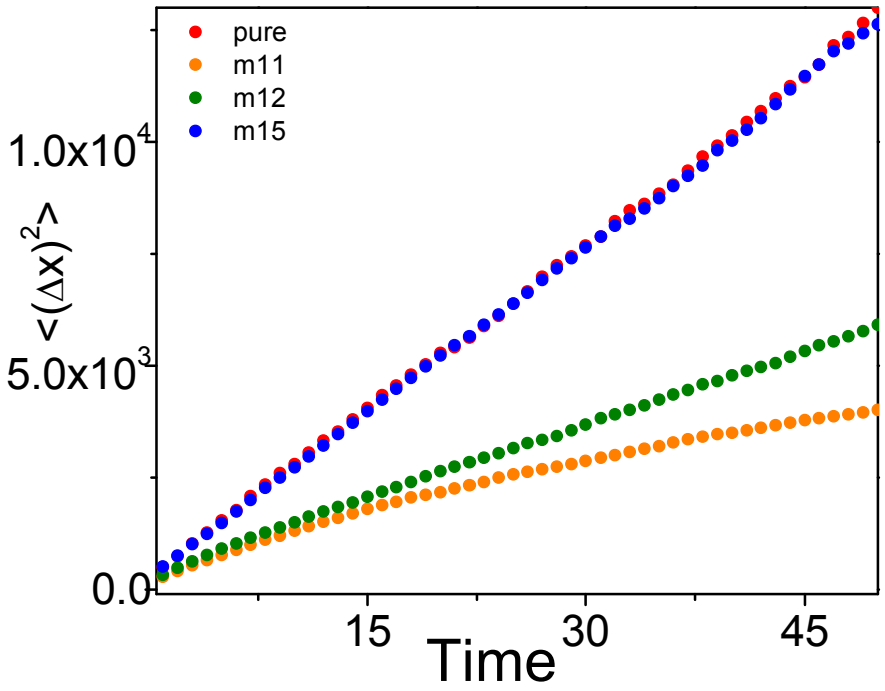

The diffusion becomes sub-diffusive as the particle diffuses through a mesh like structure. With increase in mesh structure the particle motion approaches normal diffusion. The increase in β (0> β >1) towards unity is a reflection of the transition from sub-diffusion to normal diffusion transition.

Figure 2.4.1(e)

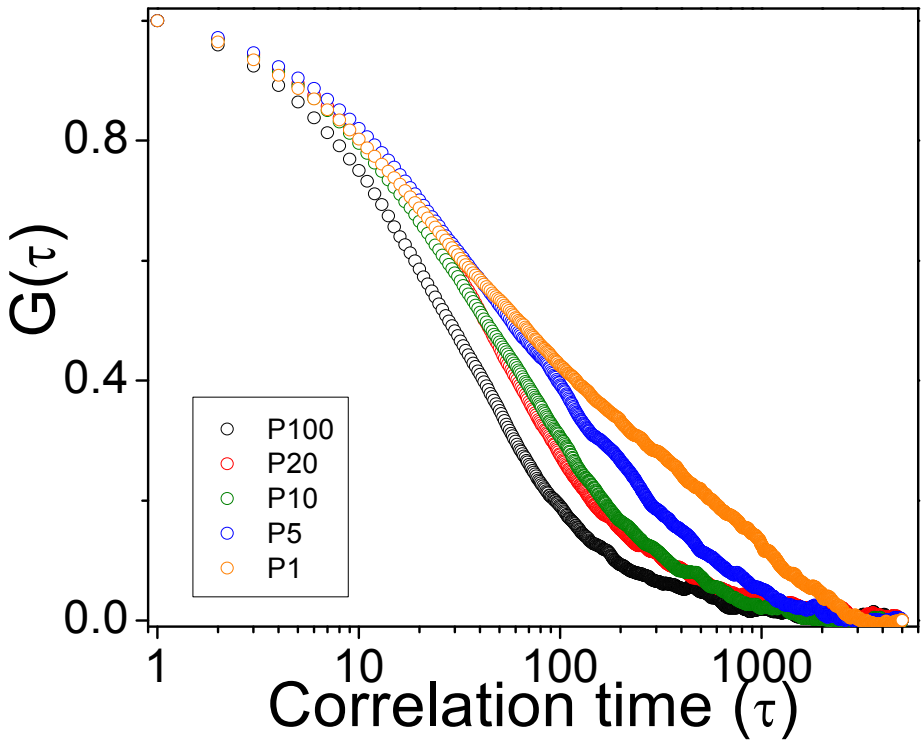

As the mesh size decreases and becomes comparable to the step size the diffusion becomes constrained which is reflected in the ACF as β decreases (β<1). Here mesh size is altered with 20% variability.

(iv). 'Diffusion with interaction'.

To understand the origins of two timescales in linker histone diffusion, the 'diffusion-with-interaction' model is used, where a few random binding sites have been numerically generated in 3D space. Here the binding coordinates are either fixed in each of the time trace or randomly varied inside the confocal volume while keeping the total number of binding sites same. Both cases give us similar simulation results.

In this simulation, the linker histones are treated as Brownian particles that undergo both 3D random diffusion and interact with dynamic pinning sites depicting chromatin structure. Each of these particles is made to undergo 40000 random steps in 3D. At the time of diffusion as the coordinate of the molecule matches with the interacting site the molecule pauses there for a certain amount of time and begins to randomly diffuse again without any memory of the location of its previous interacting site. The total number of such diffusing particles is maintained in such a way that at any given instant an average of at least one molecule crosses the confocal detection. Such a detection, in the simulation, is realized by imposing a Gaussian excitation profile with the width (σ) of the profile 30 units around the origin (0, 0, 0). Equivalent to the FCS experiment, the Brownian particle crossing through this Gaussian profile contributes to the intensity variation in the time series to obtain the autocorrelation curve. In order to relate to our linker histone mobility data, we incorporated the presence of binding sites in the simulation. **Figure 2.4.1(f)** shows the X-Y trajectory of a single Brownian particle through a randomly distributed interacting site (Red circles). As the coordinate of the particle matches with the coordinate of the interacting site, the particle pauses there for a certain time. Here we assume a single particle diffusing in an environment with a variable number of interacting sites (N = 0, 1500, 2000, 3000) in the confocal volume, where the particle binds with a mean residence time 4000 units with a gaussian distribution of width 40 %. The typical residence time has been chosen as 4000 unit to match our experimental finding that interaction dependent diffusion timescale is 100 times slower than the normal

diffusion timescale and the standard deviation in the residence time is kept 40% as the SD of our interaction timescale in the experiment is ~40%. Figure 2.4.1(g) demonstrates that as the particle enters the confocal volume, (Blue) the intensity increases sharply and after the typical diffusion timescale (τ_1) it falls back to the noise level. But in the case of diffusion with interaction, the non-interacting (τ_1) and interacting particles (τ_2) give rise to two distinct timescales in the autocorrelation function.

The results of this simulation are plotted in **Figure 2.4.1(h)**, which shows the existence of a distinct second time scale in the autocorrelation curve. We also present data where all the simulation parameters except the number of interacting sites are fixed to explain the effect of interacting sites on linker histone mobility.

Figure 2.4.1(f)

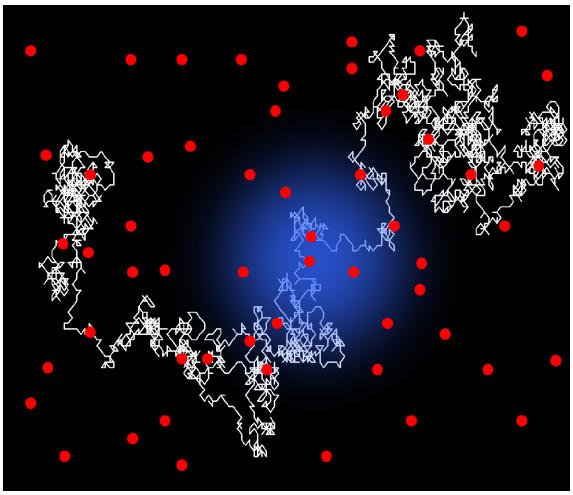

Diffusion trajectory of a particle through randomly distributed interacting sites (Red circles). The Gaussian excitation profile is shown at the center (Blue). At the time of diffusion as the coordinate of the particle matches with the coordinate of the interacting site it pauses there for a certain time.

Figure 2.4.1(g)

(i)

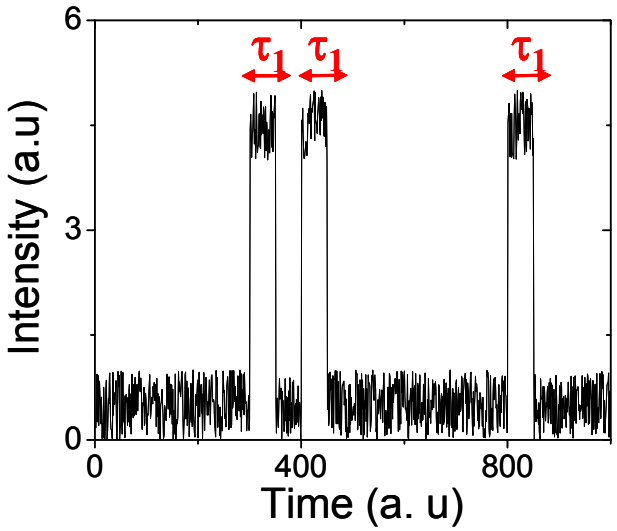

(ii)

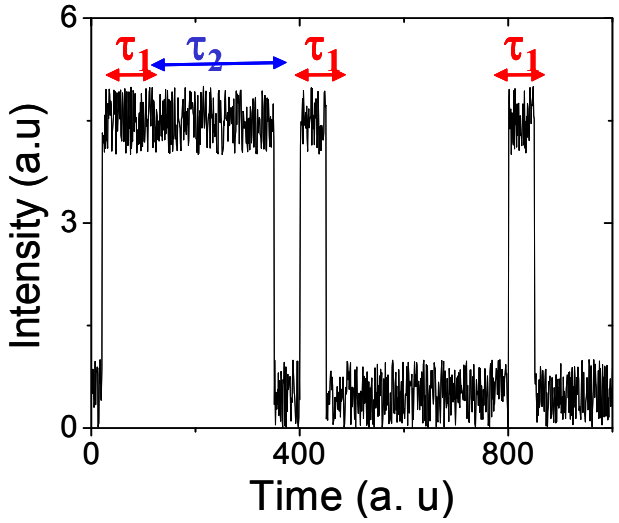

(i) Typical time-series for a particle diffusing through the confocal volume with out any interacting site and (ii) in the presence of randomly distributed interacting sites.

Figure 2.4.1(h)

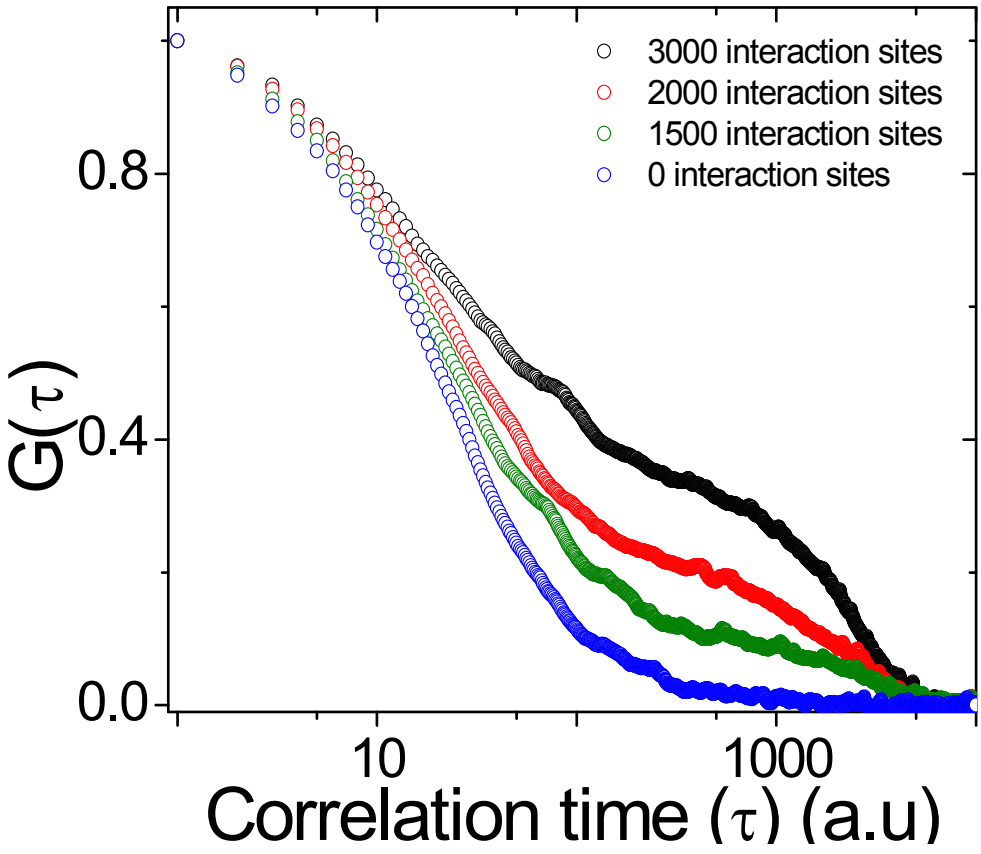

Autocorrelation function generated by numerical simulation for 3D diffusion with randomly distributed interacting sites (N = 0, 1500, 2000 & 3000).

2.5 Conclusion

Core histones are found to exchange with a $\tau_{1/2} \sim 130$ min **[22]**, while the linker histones have a $\tau_{1/2} \sim$ minutes **[16, 17]**. Most core histones are found to be associated with the chromatin and are maintained in position through mitosis. Among the free fraction of core histones, the H2A-H2B dimer exchanges more rapidly than the H3-H4 tetramer **[22]**, suggesting that the bound H3-H4 may provide stable epigenetic markers **[23]**. It is also found that replication independent dynamic exchange of the core histones are deposited to transcriptionally active sites **[24]**. The exchange of H2A and H2B is found to be mediated by processes that are ATP dependent **[19]**. In contrast, the mobility of linker histones and their subtypes is dependent on their tail residues **[18]**. Despite the existing information on histone mobility within the nucleus, the underlying mechanisms of their diffusion remain unclear.

The hindrance to histone mobility offered by the heterogeneous chromatin assembly is first established. We then show that the core histones exist in multimeric states and that their mobility is invariant across organisms. In the cytoplasm of over expressing cells, the core histones are in monomeric form, indicating that the nuclear environment is important to maintain the multimeric form of the core histones. Hence the freely diffusion of the core histones is important to maintain the epigenetic state of the cell nucleus. In contrast, the linker histone mobility shows two distinct time scales, one arising due to normal diffusion and the other due to its interactions with chromatin. The multimeric form of the core histones is ATP dependent but, the interaction timescale of the linker histones is independent of ATP concentration inside the cell nucleus. Functional perturbations to chromatin, such as ATP depletion and cell death, suggest differential roles for core and linker histone dynamics. Colocalization experiments of histones reveal spatial heterogeneity in their enrichment within living cells. The experimental results have been validated by numerical simulations.

Schematic model

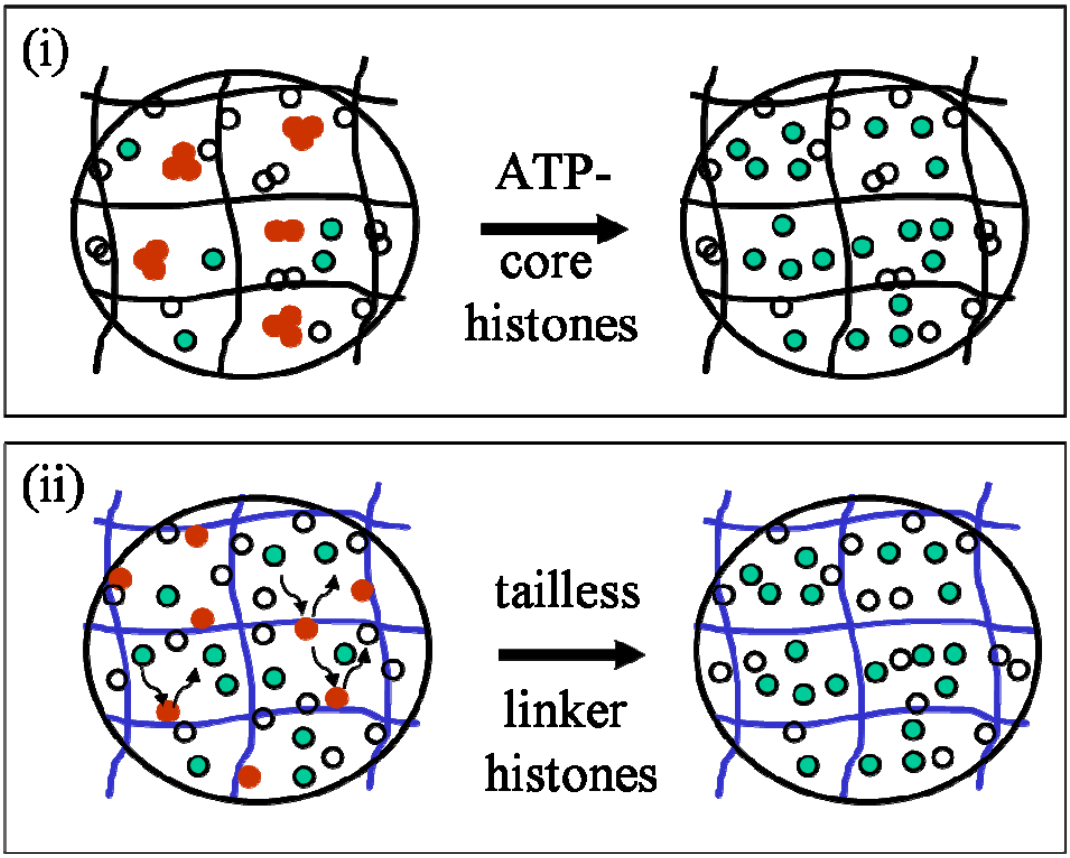

Schematic model of the mobility of (i)core and (ii) linker histones within the cell nucleus. Core histones (H2B-EGFP) remain in the multimeric form (red) in normal physiological condition. Upon ATP depletion the multimeric core histones (H2B-EGFP) become monomeric (green). Linker histones diffuse through the chromosomal mesh structure by diffusion with interaction (Red - interacting; Green - non-interacting). For tail-less linker histones the motion is purely diffusive and there is no interaction.

Table-1 Core histone diffusion

	Nucleus (ATP+)	Nucleus (ATP-)	Cytoplasm	Sorted chromosome
EGFP	26.4±2.7	26.0 ±7.9	X	X
TMR-D	19.8 ±4.9	X	X	14.8 ±8.2
ACN	7.1±3.2	8.7±4.7	X	X
H2B-EGFP	7.3±1.9	12.7±5.3	22.2 ± 5.4	X
H4-EGFP	7.3±3	10.4±4.8	X	X

Unit - $\mu m^2/sec$

Table-2 Linker histone diffusion

H1 subtypes	D_1	D_2	ATP(-) D_1	ATP(-) D_2	Cytoplasm
H1.1(H1a)	19.5±3.5	0.3±.1	X	X	X
H1.5(H1b)	25.1±4.7	0.2±.1	24.8 ± .5.7	0.2 ±0.1	16.6 ±5.5
H1.2(H1c)	24.9±3.9	0.2 ±.1	X	X	X
H1.4(H1e)	23.6±4.3	0.2±.1	X	X	X
H1.1 (tailless)	20.2 ±5.2	X	X	X	X

Unit - $\mu m^2/sec$

2.6 Reference

1. Spector, D.L., *The dynamics of chromosome organization and gene regulation.* Annu Rev Biochem, 2003. 72: p. 573-608.

2. Ahmad, K. and S. Henikoff, *Epigenetic consequences of nucleosome dynamics.* Cell, 2002. 111(3): p. 281-4.

3. Khorasanizadeh, S., *The nucleosome: from genomic organization to genomic regulation.* Cell, 2004. 116(2): p. 259-72.

4. Hansen, J.C., *Conformational dynamics of the chromatin fiber in solution: determinants, mechanisms, and functions.* Annu Rev Biophys Biomol Struct, 2002. 31: p. 361-92.

5. Becker, M., et al., *Differential in vivo binding dynamics of somatic and oocyte-specific linker histones in oocytes and during ES cell nuclear transfer.* Mol Biol Cell, 2005. 16(8): p. 3887-95.

6. Bustin, M., F. Catez, and J.H. Lim, *The dynamics of histone H1 function in chromatin.* Mol Cell, 2005. 17(5): p. 617-20.

7. Gasser, S.M., *Visualizing chromatin dynamics in interphase nuclei.* Science, 2002. 296(5572): p. 1412-6.

8. Kanda, T., K.F. Sullivan, and G.M. Wahl, *Histone-GFP fusion protein enables sensitive analysis of chromosome dynamics in living mammalian cells.* Curr Biol, 1998. 8(7): p. 377-85.

9. Banerjee, B., D. Bhattacharya, and G.V. Shivashankar, *Chromatin structure exhibits spatio-temporal heterogeneity within the cell nucleus.* Biophys J, 2006. 91(6): p. 2297-303.

10. Deepak Sinha, D.B., Bidisha Banerjee, Feroz Meeran & G.V.Shivashankar., ***Development of single molecule tracking fluorescence microscope combined with force spectroscopy for gene expression analysis.*** **Current science, 2004. 87.: p. 239-244.**

11. Pardue, M.L., ***Looking at polytene chromosomes.*** **Methods Cell Biol, 1994. 44: p. 333-51.**

12. Mangenot, S., et al., ***Salt-induced conformation and interaction changes of nucleosome core particles.*** **Biophys J, 2002. 82(1 Pt 1): p. 345-56.**

13. Yager, T.D., C.T. McMurray, and K.E. van Holde, ***Salt-induced release of DNA from nucleosome core particles.*** **Biochemistry, 1989. 28(5): p. 2271-81.**

14. Mangenot, S., S. Keller, and J. Radler, ***Transport of nucleosome core particles in semidilute DNA solutions.*** **Biophys J, 2003. 85(3): p. 1817-25.**

15. Weidemann, T., et al., ***Counting nucleosomes in living cells with a combination of fluorescence correlation spectroscopy and confocal imaging.*** **J Mol Biol, 2003. 334(2): p. 229-40.**

16. Lever, M.A., et al., ***Rapid exchange of histone H1.1 on chromatin in living human cells.*** **Nature, 2000. 408(6814): p. 873-6.**

17. Misteli, T., et al., ***Dynamic binding of histone H1 to chromatin in living cells.*** **Nature, 2000. 408(6814): p. 877-81.**

18. Th'ng, J.P., et al., ***H1 family histones in the nucleus. Control of binding and localization by the C-terminal domain.*** **J Biol Chem, 2005. 280(30): p. 27809-14.**

19. Bruno, M., et al., ***Histone H2A/H2B dimer exchange by ATP-dependent chromatin remodeling activities.*** **Mol Cell, 2003. 12(6): p. 1599-606.**

20. Khochbin, S., *Histone H1 diversity: bridging regulatory signals to linker histone function.* Gene, 2001. 271(1): p. 1-12.

21. Bhattacharya, D., et al., *EGFP-tagged core and linker histones diffuse via distinct mechanisms within living cells.* Biophys J, 2006. 91(6): p. 2326-36.

22. Kimura, H. and P.R. Cook, *Kinetics of core histones in living human cells: little exchange of H3 and H4 and some rapid exchange of H2B.* J Cell Biol, 2001. 153(7): p. 1341-53.

23. Turner, B.M., *Cellular memory and the histone code.* Cell, 2002. 111(3): p. 285-91.

24. Thiriet, C. and J.J. Hayes, *Replication-independent core histone dynamics at transcriptionally active loci in vivo.* Genes Dev, 2005. 19(6): p. 677-82.